

①

1990

THESIS/~~DISSERTATION~~

Short-Range Forecasting Using a One-Dimensional
Planetary Boundary Layer Model

Thomas J. Borland

AFIT Student Attending: Florida State University

AFIT/CI/CIA-90-149

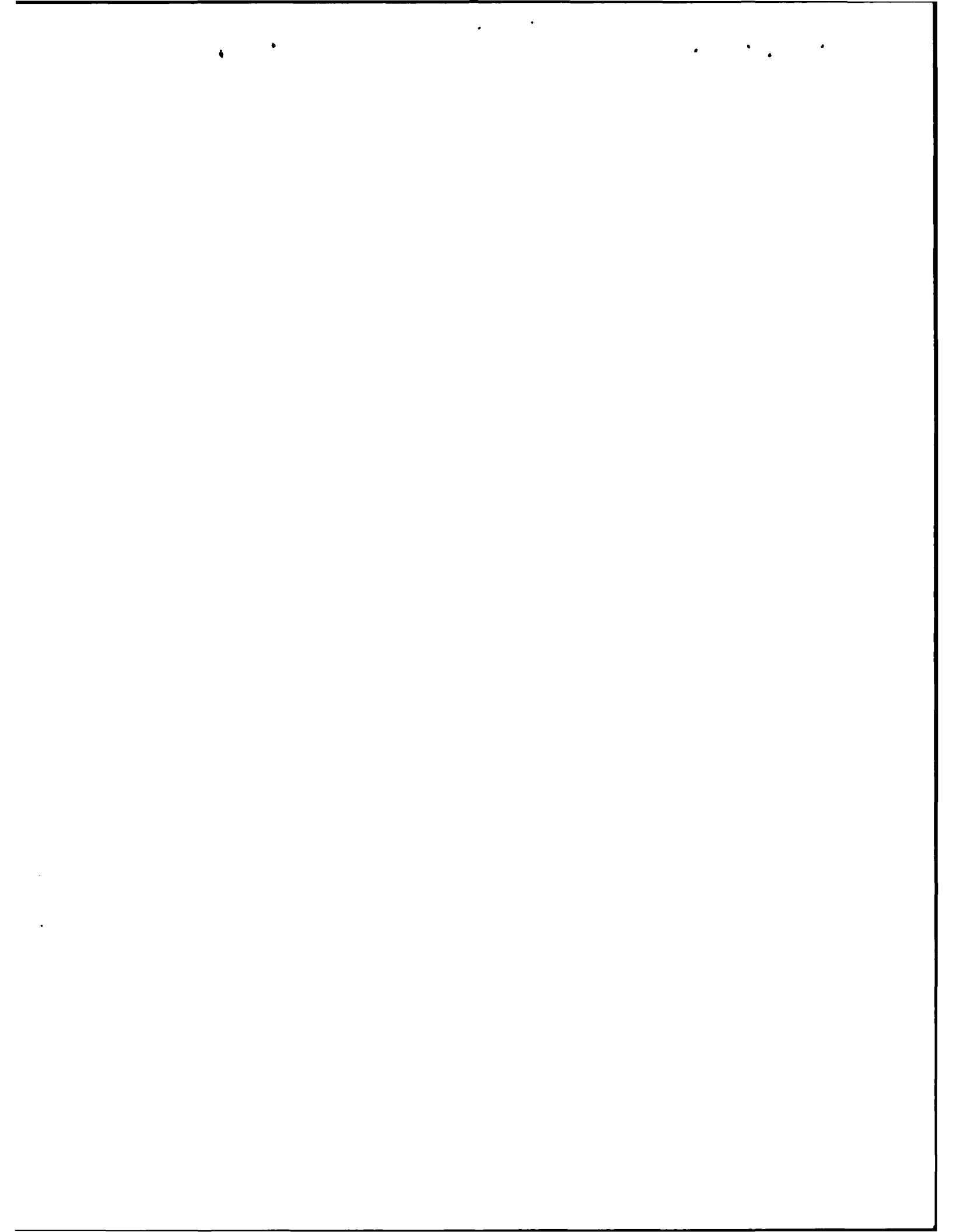
AFIT/CI
Wright-Patterson AFB OH 45433-6583

Approved for Public Release IAW 190-1
Distributed Unlimited
ERNEST A. HAYGOOD, 1st Lt, USAF
Executive Officer

DTIC
ELECTE
FEB 07 1991
S B D

AD-A231 704

AD-A231 704



THE FLORIDA STATE UNIVERSITY
COLLEGE OF ARTS AND SCIENCES

SHORT-RANGE FORECASTING USING A ONE-DIMENSIONAL
PLANETARY BOUNDARY LAYER MODEL

By

THOMAS J. BORLAND

A Thesis submitted to the
Department of Meteorology
in partial fulfillment of the
requirements for the degree of
Master of Science

Degree Awarded:

Summer Semester, 1990

The members of the committee approve the thesis of Thomas J. Borland
defended on 17 July, 1990

Paul Ruscher

Paul Ruscher
Professor Directing Thesis

N E La Seur

Ncel La Seur
Committee Member

Steven A. Stage

Steven Stage
Committee Member



Accession For	
NTIS GRA&I	<input checked="" type="checkbox"/>
DTIC TAB	<input type="checkbox"/>
Unannounced	<input type="checkbox"/>
Justification	
By _____	
Distribution/	
Availability Codes	
Dist	Avail and/or Special
A-1	

DEDICATION

This thesis is dedicated to my parents, Thomas and Margaret Borland, who always encouraged my interests in science and provided support, discipline and love.

ACKNOWLEDGEMENTS

I would like to thank the United States Air Force for providing the opportunity and the financial assistance to attend graduate school. I would also like to thank Dr. Paul Ruscher for his support, guidance and patience during my tenure at Florida State. A special thanks to my committee members Dr. Noel La Seur and Dr Stephen Stage for their suggestions. I also owe a debt of gratitude to Jeff Walker and Jimmy Hudson for answering my endless stream of computer questions.

A special thank you to Dr Henry Fuelberg and his students for the use of data tapes from the COHMEX experiment.

Finally, I wish to express my deepest appreciation to my wife, Ellen for her understanding and support and for believing in me when I didn't believe in myself. Thank you, sweetheart. I love you.

TABLE OF CONTENTS

	Page
LIST OF TABLES	vi
LIST OF FIGURES	vii
LIST OF SYMBOLS	x
ABSTRACT	xiii
CHAPTER 1. INTRODUCTION	1
CHAPTER 2. THE BOUNDARY LAYER MODEL	7
CHAPTER 3. METHODOLOGY	21
CHAPTER 4. RESULTS	33
CHAPTER 5. FUTURE IMPROVEMENTS TO MODEL	73
CHAPTER 6. CONCLUSION	80
APPENDIX	83
REFERENCES	84
BIOGRAPHICAL SKETCH	87

LIST OF TABLES

Table		Page
1	The computed values of WSOIL for Nashville, Tennessee and Redstone Arsenal for the three days examined during this work.	29
2	The variables that are changed during the four experiments .	32
3	R ² values for Nashville, Tennessee, and Redstone Arsenal, Alabama for 16 July 1986, 9 June 1986 and 17 June 1986. . .	34
4	The WXP vertical velocity as computed by the kinematic method on 12 June 1990, 0000 GMT for Nashville, Tennessee; Centreville, Alabama and Athens, Georgia.	76

LIST OF FIGURES

Figure		Page
1	The COHMEX rawinsonde network (solid lines). Nashville, Tennessee is located at BNA; Redstone Arsenal, Alabama is located at number 11.	22
2	The boundary-layer depth as a function of local standard time for water availability $b \equiv \text{surface evaporation/potential evaporation} = 0$ (open circles), 0.25 (open squares), 0.50 (solid triangles), 0.75 (open triangles), and 1.0 (solid circles). (From Troen and Mahrt, 1986).	25
3	Antecedent Retention Index values for Nashville, Tennessee (top) and Redstone Arsenal, Alabama. ARI 1 is the Antecedent Retention Index for the top soil layer (5 centimeters thick), ARI 2 is the Antecedent Retention Index for the lower soil layer (95 centimeters thick). June 1 is Julian day 152, and July 29 is Julian day 210.	28
4	NMC surface analysis for 1200 GMT 9 June 1986.	37
5	NMC 50 kPa analysis for 1200 GMT 9 June 1986	38
6	The planetary boundary layer height in meters (top), and the Bowen ratio (bottom) for Redstone Arsenal, Alabama; 1200 GMT, 9 June 1986. CRG, experiment A; ARI, experiment B; NS, experiment C; WILT, experiment D.	39
7	Temperature and dew-point temperature traces with forecast two meter temperature and dew-point temperature trace for Redstone Arsenal, Alabama, 9 June 1986.	41
8	Surface energy balance for Redstone Arsenal, Alabama 9 June 1986.	42
9	The planetary boundary layer height in meters; and the Bowen ratio for Nashville, Tennessee; 1200 GMT, 9 June 1986.	44
10	Temperature and dew-point temperature traces with forecast two meter temperature and dew-point temperature traces for Nashville, Tennessee, 1200 GMT 9 June 1986.	45
11	NMC 50 kPa analysis 1200 GMT 16 July 1986.	47

12	NMC surface analysis 1200 GMT 16 July 1986.	48
13	The planetary boundary layer height in meters and the Bowen ratio for Redstone Arsenal, 1200 GMT, 16 July 1986.	49
14	Temperature and dew-point temperature traces with forecast two meter temperature and dew-point temperature traces for Redstone Arsenal, Alabama, 1200 GMT, 16 July 1986.	50
15	Forecast PBL height and Bowen ratio for Nashville, Tennessee on 16 July 1986.	52
16	Actual and forecast temperature and dew-point temperature traces for Nashville, Tennessee, 16 July 1986.	54
17	Surface isodrosotherm analysis (1°C intervals) every 30 min from 1600 to 1830 GMT based on COHMEX data. (Schudalla 1988).	56
18	NMC surface analyses for 1200, 1500, and 1800 GMT 17 June 1986 (Schudalla, 1988).	57
19	Forecasted PBL heights for Nashville and Redstone Arsenal for 17 June 1986.	59
20	Bowen ratio for Redstone Arsenal and Nashville for 17 June 1986.	61
21	Surface energy balance for Redstone Arsenal and Nashville for 17 June 1986.	63
22	Actual and forecast temperature and dew-point temperature for Redstone Arsenal and Nashville for 17 June 1986.	64
23	Comparison of forecasted dew-point temperature runs to actual dew-point temperature for 17 June 1986 at Nashville, Tennessee.	66
24	Forecast PBL cloud cover at Nashville and Redstone Arsenal for 9 June, 17 June, and 16 July for experiments A and B.	68
25	Forecast solar radiation for Redstone Arsenal for 9 June 1986.	69
26	Forecast solar radiation for Redstone Arsenal for 16 July 1986.	70
27	Forecast values of solar radiation and PBL cloud cover for 9 June at Nashville, Tennessee and 17 June at Redstone Arsenal, Alabama.	72

28	Vertical profile of the advection of mixing ratio by the observed wind at 36.2° north, 86.7° west (Nashville, Tennessee) as computed by the GDPROF program of the GEMPAK meteorological data display system.	77
29	Vertical profile of the advection of temperature by the observed wind at 36.2° North, 86.7° west (Nashville, Tennessee) as calculated by the GDPROF program of the GEMPAK meteorological data display system.	78
30	Vertical profile of the advection of momentum by the observed wind at 36.2° north, 86.7° west (Nashville, Tennessee) as calculated by the GDPROF program of the GEMPAK meteorological data display system.	79

LIST OF SYMBOLS

2.1 - Boundary Layer model

γ - counter gradient term

$(w'\theta')_s$ - surface flux of potential temperature

h - boundary layer depth

w_s - velocity scale ($m\ s^{-1}$)

u^* - friction velocity

z_s - top of surface layer ($0.1\ h$)

L - Monin - Obukhov length

ϕ_m - non-dimensional profile function (shear)

K_m - coefficient of diffusivity for momentum

K_h - coefficient of diffusion for heat

Pr - Prandtl number

k - Von Kármán constant (0.40)

ϕ_h - nondimensional profile function (temperature)

z_i - boundary layer height

Ri_{cr} - critical Richardson number

θ_{ov} - reference virtual potential temperature at the first model layer above the surface

θ^{*ov} - low level potential temperature

$\theta_v(h)$ - the virtual potential temperature at model level h

2.2 - Surface layer model

u^*2 - momentum flux

$(w'\theta')_s$ - heat flux

$(w'q')_s$ - moisture flux

C_m - surface exchange coefficient for momentum

C_h - surface exchange coefficient for heat

Ri_b - bulk Richardson number

z_{om} - roughness length for momentum

z_{oh} - roughness length for heat

θ_{sv} - surface virtual potential temperature

$(w'\theta'_v)_s$ - virtual potential temperature flux at the surface

2.3. - Soil - Canopy model

Θ - volumetric water content

$D(\Theta)$ - coefficient of diffusivity

$K(\Theta)$ - hydraulic conductivity

E_{dir} - direct evaporation at air-soil interface

I - infiltration rate

σ_f - shading factor

E_p - potential evaporation

C^* - canopy water content

E_c - canopy evaporation of water

k_v - non-dimensional plant resistance factor

- E_t - transpiration
- q_s - surface specific humidity
- $C(\Theta)$ - volumetric heat capacity of soil
- $K_T(\Theta)$ - thermal conductivity of soil
- G - soil heat flux

2.4 - Surface energy balance

- $S\downarrow$ - downward solar radiation (positive downward)
- $L\downarrow$ - downward atmosphere radiation (positive downward)
- $\sigma\theta_s^4$ - downward terrestrial radiation (positive downward)
- θ_s - surface potential temperature
- G - soil heat flux
- H - sensible heat flux
- $L\cdot E$ - latent heat flux
- α - albedo

SHORT-RANGE FORECASTING USING A ONE-DIMENSIONAL PLANETARY BOUNDARY LAYER MODEL

Thomas J. Borland, M.S.
The Florida State University, 1990
Major Professor: Paul H. Ruscher, Ph. D.

An investigation of a one-dimensional planetary boundary layer model is performed to test its ability to accurately predict temperature and dew-point temperature for a 12 hour period. The model is initialized using upper-air sounding data on three separate cases. For each case, four experiments are run to determine which parameters are most critical in providing the best forecast results. These tests include changing the values of soil moisture, running the model with a different soil type and lowering the value of the wilting point.

The default parameter tests showed extremely good results for temperature; however, the results for dew-point temperature were highly variable and quite often poor. This motivated the development of an antecedent retention index (ARI) to compute soil moisture. The tests performed with the ARI improved the dew-point temperature forecasts dramatically. Also examined are the sensitivity of boundary layer height, cloud cover, and model surface energy balance output to soil moisture content. The models temperature and dew-point temperature forecasts could be used for air mass

thunderstorm forecasting. Future applications of the model include the incorporation of vertical velocity and the advection of temperature, moisture and momentum from software available at FSU.

CHAPTER 1

INTRODUCTION

Scattered air mass thunderstorms can often be found over the southeastern United States during the months of May through September. The problem an operational meteorologist has during this time of year is to pinpoint where these storms will occur. As noted in McGinley (1986) four elements are essential in the formation of convection:

- (1) a moist layer near the ground
- (2) convective instability
- (3) a stable layer or cap acting as a
restraining influence
- (4) a trigger mechanism

During the summer months the moist, southerly flow from the west side of the Bermuda High dominates the weather of the southeastern United States and provides the first two elements. While a subsidence inversion from the Bermuda High may provide the restraining influence, it is usually provided by an inversion created by nighttime radiational cooling. The most difficult problem for the forecaster is the determination of the trigger mechanism.

The trigger mechanisms which initiate convection have been determined as processes that will induce upward vertical motions. These may

include fronts (cold or warm), upper level divergence, surface heating, topographically forced circulations or sea breezes acting individually or in any combination. With the position of the polar jet stream along the U.S.-Canadian border during the summer, most of the usual trigger mechanisms are non-existent. For example, most 50 kPa (500 millibar) short wave features associated with upper level divergence are well to the north of the southeastern United States and as a result, the surface low-pressure systems and their associated fronts are also to the north. Therefore, in this case the most logical trigger mechanism would be surface heating. The problem encountered by the forecaster is how much solar heating is needed to lift the air at the surface above the inversion. This can be determined with the aid of a vertical sounding and a skew-T/ln-p diagram.

How the temperature of air changes with height has been investigated for about 100 years. Recordings of temperature changes on manned balloons were first done in the 1890's. Recordings with kites were done in the 1920's (La Seur, personal communication 1989). It wasn't until 1935 that the first serial ascent with the use of recording instruments tied to weather balloons was attempted over Europe (Bjerknes & Palmén 1937). This was the first attempt to determine the large scale vertical structure of the atmosphere.

After World War II the launching of radiosondes became commonplace. Fawbush & Miller's (1952) landmark study on soundings that were representative of a tornadic environment led the way in the use of soundings as a forecast tool for severe weather at a specific location. Over the next several years stability parameters were derived from soundings that gave an

indication of how stable or unstable a particular air mass might be on a given day. These indices include the K-Index, Lifted Index and Total-Totals. While these methods give a relative idea of how potentially unstable an air mass is, they give no real indication of a thunderstorm will form.

Atmospheric soundings are taken at 0000 Greenwich Mean Time (GMT) and 1200 GMT. From these soundings we can determine the temperature and moisture values in the early morning and early evening for a particular sounding station. However, many thunderstorms develop between these time periods. Several methods have been developed to try and determine from a 12 GMT sounding if thunderstorms would form within a 12 hour period. One method used by many forecasters is simply to determine the convective temperature; the surface temperature needed to initiate convection. This is done by compressing an air parcel at the convective condensation level (CCL) dry adiabatically to the surface and determine the temperature. While this is a simple process it is not very effective.

Another method is suggested by McGinley (1986). By this method, 'boxes' are formed by the intersection of dry adiabats (at 2° C intervals) and isotherms (at 1° C intervals). In this convention one 'box' equals 7 J/Kg. The cumulative number of boxes by hour can be roughly estimated by the formula

$$E(t) = E_t \frac{[1 - \cos((t - t_r) / T_g)]}{2} \quad (1)$$

where t is the current time, E is the input energy, E_t is the total input energy, t_r is

sunrise time and T_s is total sunhours. E_t can be modified by coefficients responding to cloud cover, haze and surface moisture. McGinley points out that "these rough estimates work well for the southern plains", while no mention is made on how this method of computing would work for the southeastern U.S. One possible reason for the success of this method for the southern plains is the effect of warm, dry air from the Sierra Madre Oriental mountains of Mexico that provide a strong capping inversion, while the southeastern U.S. is too far away to feel the effects of these winds as most soundings during the summer are saturated through a greater vertical extent than those in the plains.

What can be gained from using the forecast products from the National Meteorological Center (NMC) to forecast thunderstorms? Since air mass thunderstorms are a mesoscale phenomenon, they will be too small to be resolved on the grid used in the Nested Grid Model (NGM) that is prepared by the NMC. According to Hoke (1989), moist convection occurs at a model grid point when 1) there is convergence of moisture in the bottom six layers of the model, 2) a parcel originating in any of the lowest four layers of the model would become buoyant or lifted (convective instability) and 3) total moisture convergence into the column below the cloud top is positive. Therefore, the NGM would be of little use for a specific spot to a forecaster in the southeastern U.S. during the summer.

These short range forecasting tools all have various strengths and weaknesses. It is my contention that a better method of forecasting air mass thunderstorms can be found by using a one dimensional PBL layer model to

determine the fluxes of heat and moisture in the atmosphere as well as the effects of the soil and plant canopy. In particular a model could be used to compute the hourly evolution of the planetary boundary layer and from this, the shelter temperature and dew-point temperature. The T and T_d forecasts could then be used in a surface stability index, such as a surface-based lifted index.

As a first step toward this ultimate goal, we will attempt to forecast hourly T and T_d and verify these forecasts for locations in the southeastern U.S. The one-dimensional model that will be used in this study (OSU1DPBL) was originally developed by Troen & Mahrt (1986) as the boundary layer formulation in a large-scale NWP model (Brenner, et al., 1988). This model incorporates an interactive soil layer and a plant canopy model in addition to a PBL model. This will provide an estimate of the surface energy balance that will include the effects of surface heating, evaporation and transpiration. The model is capable of calculating u & v components of wind, temperature and moisture parameters and fluxes of heat, moisture & momentum throughout the depth of the PBL as a function of turbulent diffusion. Output produced also includes the height of the boundary layer, and surface parameters such as air temperature & humidity at 2 meters, anemometer-level winds, the surface energy balance and soil temperature and moisture.

The purpose of this study is to determine if a modified version of the one-dimensional model of Troen & Mahrt can be used to provide guidance such as hourly T and T_d . This ultimately could prove useful for forecasting the occurrence of airmass thunderstorms in the absence of large-scale forcing. The primary data set is from the Cooperative Huntsville Mesoscale Experiment

(COHMEX) of 1986. Specifically, the study will examine data from several days during the experiment with several objectives: 1) examine how well the model forecasts temperature and dew-point temperature during a 12 hour period, 2) develop a soil moisture index and test the sensitivity of the model temperature and dew-point temperature forecasts to soil moisture input and 3) attempt to determine how the evolution of the PBL may affect the formation of air-mass thunderstorms.

The second chapter will examine the OSU1DPBL model and the computational procedures. Readers who do not wish to investigate the exact details of the model may skip this chapter. The third chapter addresses the methodology behind the experiments and the development of an antecedent retention index for the soil. Chapter four reveals the results of the study, while chapter five discusses some future related applications of the model and chapter six draws conclusions of this study.

CHAPTER 2

THE BOUNDARY LAYER MODEL

This chapter will describe the equations that are used in the OSU1DPBL model used during this study. The computational procedures and a flow chart can be found in Ek and Mahrt (1989). The model was initially developed for use as the boundary layer formulation of the global spectral model of the U.S. Air Force Geophysical Laboratory.

2.1 Boundary layer model

The model forecasts the tendencies due to turbulent mixing of the potential temperature (θ), specific humidity (q), and horizontal components of the wind (\vec{V}_h , or u and v) (Ek and Mahrt, 1989). The set of prognostic equations is

$$\frac{\partial \vec{V}_h}{\partial t} = \frac{\partial}{\partial z} \left(K_m \frac{\partial \vec{V}_h}{\partial z} \right) - w \left(\frac{\partial \vec{V}_h}{\partial z} \right) - f \hat{k} \times \vec{V}_g \quad (2)$$

$$\frac{\partial \theta}{\partial t} = \frac{\partial}{\partial z} \left(K_h \left(\frac{\partial \theta}{\partial z} - \gamma_\theta \right) \right) - w \left(\frac{\partial \theta}{\partial z} \right) \quad (3)$$

$$\frac{\partial q}{\partial t} = \frac{\partial}{\partial z} \left(K_h \frac{\partial q}{\partial z} \right) - w \left(\frac{\partial q}{\partial z} \right) \quad (4)$$

Here, only the vertical diffusion terms due to boundary layer turbulent mixing, and the advection terms due to a prescribed vertical motion field are kept in the equations. This is because other forcing terms normally found in these equations (Holton, 1979) would be given by the large-scale NWP model. Their neglect here limits the situations that the model may be used for. This point will be addressed again in later chapters. Details of the complete equations may be found in Troen and Mahrt (1986).

The counter-gradient correction for potential temperature (γ) is included in (3) following Troen and Mahrt (1986), and is parameterized as follows

$$\gamma\theta = \begin{cases} 0 & , \text{ stable} \\ C \frac{\overline{(w'\theta')_s}}{w_s h} & , \text{ unstable} \end{cases} \quad (5)$$

The counter-gradient correction is evaluated in terms of the surface flux of potential temperature (fluxes will be described in section 2.1.2), The boundary-layer depth (h), the velocity scale (w_s) of the boundary layer defined as

$$w_s = u_* \phi_m^{-1} \left(\frac{z_s}{L} \right) \quad (6)$$

and a non-dimensional constant C , set to 8.5, as in Holtslag and Beljaars (1988), modified from the value of 6.5 in Troen and Mahrt (1986). In (6), u_* is the surface friction velocity, z_s is the top of the surface layer (currently 0.1h in the model), and L is the Monin-Obukhov length; u_* and L will also be described in section 2.2. ϕ_m is the non-dimensional profile function which is specified in (12) below. In the neutral limit as $L \rightarrow \pm \infty$, the velocity scale $w_s \rightarrow u_*$. The

coefficient of diffusivity for momentum (K_m) in the unstable case is

$$K_m = w_s h k \frac{z}{h} \left(1 - \frac{z}{h}\right)^p \quad (7)$$

with p set equal to 2.0, and $u_* \phi^{-1}(z/L)$ replacing w_s in the stable case. The eddy diffusivity for heat (K_h) is related to the eddy diffusivity for momentum in terms of the turbulent Prandtl number (Pr , non-dimensional)

$$K_h = K_m Pr^{-1} \quad (8)$$

where for the unstable case

$$Pr^{-1} = \frac{\phi_h\left(\frac{z_s}{L}\right)}{\phi_m\left(\frac{z_s}{L}\right)} + C k \frac{z_s}{h} \quad (9)$$

and is determined as the value at the top of the surface layer ($z_s = 0.1h$) using surface layer similarity theory. For the stable and neutral cases the Prandtl number is assumed to be a constant (currently 1.0 in the model).

As shown in Eq. 9, the counter-gradient term occurring in the heat equation is also absorbed in the Prandtl number. The non-dimensional profile functions (ϕ_m and ϕ_h) have their normal definition and will be defined formally below. The resulting prediction equation for the potential temperature will not explicitly contain the counter-gradient term and are actually identical in form to Eq. 2 (Troen and Mahrt, 1986).

The boundary layer height (h) is diagnosed as

$$h = \frac{Ri_{cr} \theta_{ov} |V(h)|^2}{g (\theta_v(h) - \theta_{ov}^*)} \quad (10)$$

where Ri_{cr} (non-dimensional) is the critical Richardson number, θ_{ov} is the reference virtual potential temperature at the first model height above the surface, g is the gravitational acceleration, $\theta_v(h)$ is the virtual potential temperature at model level h (currently 60 meters for the unstable case, and the first model level above the surface for the stable case), and $V(h)$ is the horizontal wind velocity at level h (the first model level above the surface). This approach to diagnosing the PBL height also requires the specification of a low-level potential temperature (θ_{ov}^*). We define θ_{ov}^* in the following way

$$\theta_{ov}^* = \begin{cases} \theta_{ov} & , \text{ stable} \\ \theta_{ov} + C \frac{\overline{(w'\theta_v')}_s}{w_s} & , \text{ unstable} \end{cases} \quad (11)$$

When the boundary layer is unstable, the virtual potential temperature at the top of the surface layer in (11) is enhanced by thermal effects, by an amount that is proportional to the surface sensible heat flux. In the neutral limit as $w_s \rightarrow u_*$, the correction to the surface temperature vanishes so that $\theta_{ov}^* \rightarrow \theta_{ov}$ and then the modified bulk Ri number (in 10) reduces to the usual one.

The non-dimensional profile functions for the shear and temperature gradients are defined as follows

$$\phi_m = \begin{cases} 6.0 & , \text{ very stable} \\ 1.0 + 5.0 z/L & , \text{ stable} \\ (1.0 - 15 z/L)^{-1/3} & , \text{ unstable} \end{cases} \quad (12)$$

and

$$\phi_h = \begin{array}{ll} 6.0 & , \text{ very stable} \\ 1.0 + 5.0 z/L & , \text{ stable} \\ (1.0 - 15z/L)^{-1/3} & , \text{ unstable} \end{array} \quad (13)$$

These forms are taken from Businger *et al.* (1971) with modifications by Holtslag and Beljaars (1988), and are functions of the height coordinate (z) and the Monin-Obukhov length scale (L). For the very stable case ($z/L > 1.0$), we set $z/L = 1.0$ so that the profile functions remain constant (following Ruscher, 1988).

2.2 Surface layer model

The surface fluxes are calculated and are parameterized following Mahrt (1987) for the stable case and Louis (1979) for the unstable case with modifications by Holtslag and Beljaars (1988) as follows

$$u_*^2 = C_m |V_0|^2 \quad (14)$$

$$\overline{(w'\theta')}_s = C_h (\theta_s - \theta_0) \quad (15)$$

$$\overline{(w'q')}_s = C_h (q_s - q_0) \quad (16)$$

Where C_m and C_h are the surface exchange coefficient for momentum and heat, respectively, and are defined so that the wind speed factor is absorbed in them. $|V_0|$ is the wind speed evaluated at the first model level above the surface.

The potential temperature (θ_0) and specific humidity (q_0) are taken at the first model level above the surface while the surface potential temperature (θ_s)

and specific humidity (q_s) are obtained from the surface energy balance.

The surface exchange coefficients are

$$C_m = k^2 |V_0| \frac{F(z, z_{0M}, Ri_B)}{\left(\ln\left(\frac{z}{z_0}\right)\right)^2} \quad (17a)$$

$$C_h = \frac{k^2}{R} |V_0| \frac{G(z, z_{0M}, z_{0H}, Ri_B)}{\ln\left(\frac{z}{z_{0M}}\right) \ln\left(\frac{z}{z_{0H}}\right)} \quad (17b)$$

where k is the non-dimensional von Kármán constant (0.40) and R , estimated at 1.0, is the ratio of the drag coefficients for momentum and heat in the neutral limit and is taken from Businger et al. (1971) with modification by Holtslag and de Bruin (1988). F and G are parameterizations of the bulk Richardson number that depend upon the stability of the PBL (Ek and Mahrt, 1989).

C_m and C_h are functions of the wind speed evaluated at the first model level above the surface ($|V_0|$), height of the first model layer above the surface (z), the roughness length for momentum (z_{0M}) which depends on surface characteristics, and the bulk Richardson number for the surface layer (Ri_B), which is described later. In addition, C_h is also a function of the roughness length for heat (z_{0H}).

The bulk Richardson number for the surface layer is defined as

$$Ri_B = \frac{g z (\theta_{0v} - \theta_{sv})}{\theta_{0v} |V_0|^2} \quad (18)$$

The bulk-Richardson number is a function of the height (z), the difference between the virtual potential temperature of air at the first model level (θ_{0v}) and

the surface virtual potential temperature (θ_{sv}) corresponding to the surface temperature from the surface energy balance, and the air speed at the first model level (V_0).

The length scale for the surface layer is the Monin-Obukhov length

$$L = - \frac{\theta_{sv} u_*^3}{g k (w'\theta'_v)_s} \quad (19)$$

The Monin-Obukhov length scale (L) is defined using the surface virtual potential temperature (θ_{sv}), friction velocity (u_*), and the virtual heat flux at the surface, and is used in the non-dimensional profile functions described in Eqs. 12 and 13.

The tendency equations for the surface layer are the same as those for the boundary layer (Eqns. 2, 3, and 4), except that the eddy diffusivities for the surface layer are

$$K_m = u_* k z \phi_m^{-1} \left(\frac{z}{L}\right) \left(1 - \frac{z}{h}\right)^p \quad (20)$$

$$K_h = K_m Pr^{-1} \quad (21)$$

where the dimensionless function ϕ_m was defined in Eq. 12. As a modification to surface layer similarity theory, the term $(1 - z/h)^p$ remains in K_m for proper matching with the mixed layer.

The only variables needed to close the surface layer model are q_s and θ_s ; these are available from the soil model (2.3) and the surface energy balance calculation (2.4), respectively.

2.3 Soil model

The soil model has been described previously by Mahrt and Pan (1984), and Pan and Mahrt (1987). The soil hydrology is modeled with the prognostic equation for the non-dimensional volumetric water content (Θ) (Ek and Mahrt, 1989).

$$\frac{\partial \Theta}{\partial t} = \frac{\partial}{\partial z} \left(D(\Theta) \frac{\partial \Theta}{\partial z} \right) + \frac{\partial K(\Theta)}{\partial z} \quad (22)$$

The coefficient of diffusivity (D) and hydraulic conductivity (K) are functions of the volumetric water content (Mahrt and Pan, 1984). Through the extremes of wet and dry soil conditions, the coefficients D and K can vary by several order of magnitude and therefore cannot be treated as constant. The layer integrated form of (24) for the i^{th} layer is

$$\Delta z_i \frac{\partial \Theta}{\partial t} = \left(D(\Theta) \frac{\partial \Theta}{\partial z} + K(\Theta) \right)_{z_{i+1}} - \left(D(\Theta) \frac{\partial \Theta}{\partial z} + K(\Theta) \right)_z \quad (23)$$

Eq. 23 is valid for a layer $[z_i, z_{i+1}] = \Delta z_i$. At the surface of the soil the evaporation is called the direct evaporation. For direct evaporation (E_{dir}) at the air-soil interface ($z=0$), we have

$$E_{\text{dir}} = \left[-D(\Theta) \left(\frac{\partial \Theta}{\partial z} \right)_0 - K(\Theta_0) \right] (1 - \sigma_f) + I (1 - \sigma_f) \quad (24)$$

where I is the infiltration rate, which is equal to zero since no precipitation is input during this work, and σ_f (in these experiments a value of 0.7) is the plant shading factor. The evaporation (E) can proceed at a potential rate (E_p) when

the apparent soil moisture at the surface (Θ_{sfc}) is greater than the air dry value (Θ_d), that is when the soil is sufficiently wet. When the soil dries out, the evaporation can only proceed at the rate that the soil can diffuse water upward from below, in which case $\Theta_{sfc} = \Theta_d$ and $E < E_p$.

The canopy evaporation of free water (E_c) is formulated as

$$E_c = E_p \sigma_f \left(\frac{C^*}{S} \right)^n \quad (25)$$

where S , the saturation water content for a canopy surface, is a constant usually chosen to be 0.002 meters, and n (non-dimensional) is taken to be 0.5 (Pan and Mahrt, 1987). The canopy water content (C^*) changes as

$$\frac{dC^*}{dt} = \sigma_f P - E_c \quad (26)$$

Precipitation (P) increases the canopy water content first while evaporation decreases C^* . The model also incorporates transpiration (E_t) in the following manner

$$E_t = E_p \sigma_f k_v \frac{\sum_{i=1}^2 [\Delta z_i g(\Theta_i)] \left[1 - \left(\frac{C^*}{S} \right)^n \right]}{\sum_{i=1}^2 [\Delta z_i]} \quad (27)$$

where k_v is the non-dimensional plant resistance factor or plant coefficient (PC), set at 0.7 for these experiments.

Total evaporation is obtained by adding the direct soil evaporation, the transpiration and the canopy evaporation

$$E = E_{dir} + E_c + E_t \quad (28)$$

The total evaporation cannot exceed the potential evaporation (Ek and Mahrt, 1989). After obtaining the evaporation, the "surface specific humidity" q_s is calculated from

$$q_s = q_0 + \frac{E}{\rho_0 C_h} \quad (29)$$

This quantity is the specific humidity at the surface which allows E to be calculated from the bulk aerodynamic relationship; q_s is also used in the calculation of vertical profiles of moisture. ρ_0 is the air density at the surface, and C_h is the exchange coefficient for heat (or moisture), described earlier.

Soil thermodynamics are treated with a prognostic equation for soil temperature (T)

$$C(\Theta) \frac{\partial T}{\partial t} = \frac{\partial}{\partial z} \left(K_T(\Theta) \frac{\partial T}{\partial z} \right) \quad (30)$$

The volumetric heat capacity (C) and the thermal conductivity (K_T) of the soil are both functions of the soil water content (Θ). While the heat capacity (C) is linearly related to Θ , the coefficient of thermal diffusivity (K_T) is a highly nonlinear function of Θ and increases by several orders of magnitude from dry to wet soil conditions. The layer-integrated form of (30) for the i^{th} layer is

$$\Delta z_i C(\Theta_i) \frac{\partial T_i}{\partial t} = \left(K_T(\Theta) \frac{\partial T}{\partial z} \right)_{z_{i+1}} - \left(K_T(\Theta) \frac{\partial T}{\partial z} \right)_z \quad (31)$$

The upper boundary condition for the soil thermodynamic model is the soil heat flux, G ($W m^{-2}$), an important component in the surface energy balance. It is found from

$$G = K_T (\Theta) \left(\frac{\partial T}{\partial z} \right)_{z=0} \quad (32)$$

The soil system is closed except for the potential evaporation, which is defined in the next section. For the two-level soil model, at 2.5 cm, the upper boundary condition is

$$\left(\frac{\partial T}{\partial z} \right)_{z=0} = \frac{\theta_s - T_{1\text{soil}}}{\Delta z} \quad (32a)$$

2.4 Surface energy balance

Surface temperature is calculated and determined from the surface energy balance method (Ek and Mahrt, 1989)

$$(1-\alpha)S\downarrow + L\downarrow - \sigma\theta_s^4 = G + H + L\cdot E \quad (33)$$

Where each term is expressed in $W\ m^{-2}$. The first term in the left-hand side of Eq. 36 is the downward solar radiation (defined as positive downward). The non-dimensional coefficient α is the surface albedo and is a function of surface characteristics. The second term on the left-hand side is the downward atmospheric radiation (positive downward). The third term on the left-hand side is the upward terrestrial radiation (positive upward); the coefficient σ is the Stefan-Boltzmann constant ($5.6696 \times 10^{-8}\ W\ m^{-2}\ K^{-4}$), and θ_s is the surface potential temperature. The first term on the right-hand side of Eq. 33 is the soil heat flux (positive downward) defined in Eq. 32. The second term on the right-hand side is the sensible heat flux (positive upward). It is defined as

$$H = \rho_0 C_p C_h (\theta_s - \theta_0) \quad (34)$$

and is a function of the air density (ρ_0), the specific heat for air ($C_p = 1004.5 \text{ J kg}^{-1} \text{ K}^{-1}$), the exchange coefficient (C_h , Eq. 17), and the difference between the surface potential temperature (θ_s) and the air potential temperature at the first model level (θ_0). The last term on the right-hand side of Eq. 33 is the latent heat flux (positive upward), where L is the latent heat of phase change; E is calculated from Eq. 28.

The potential evaporation is needed to compute the actual evaporation from (28). As a first step, the surface energy balance for the reference state of the surface (with the same albedo) is evaluated, but in a saturated condition

$$(1-\alpha)S\downarrow + L\downarrow - \sigma\theta_s'^4 = G + H' + L \cdot E_p \quad (35)$$

where

$$E_p = \rho_0 C_h (q_s^*(\theta_s') - q_0) \quad (36)$$

and

$$H' = \rho_0 C_p C_h (\theta_s' - \theta_0) \quad (37)$$

The temperature variable (θ_s') that appears in Eqs. 35-37 is a fictitious temperature that the surface would have if the soil is sufficiently wet to evaporate at the potential rate and H' is the value of sensible heat flux that would exist at θ_s' . The variable $q_s^*(\theta_s')$ in (36) is the saturation specific humidity for this fictitious temperature.

2.5 Boundary layer clouds

Fractional cloud cover in the boundary layer is calculated by using the generalized equation (Ek and Mahrt, 1989)

$$CLC = \left(\frac{RH - RH_{crit}}{1 - RH_{crit}} \right)^p \quad (38)$$

where CLC is the fractional cloud cover, RH is the environmental relative humidity explained below, RH_{crit} is the critical relative humidity for the onset of clouds, and p is an empirically derived exponent.

For the stable case Eq. 38 is taken using the maximum RH in the lowest 2000 meters of the model, with $RH_{crit}=0.8$ and $p=2$, that is, stable clouds (i.e. stratus) form when the RH is greater than 80% somewhere in the lowest 2 km of the model. For the unstable case, fractional cloud cover is the maximum of the above formulation used for the stable case, and Eq. 38 using the environmental RH at the surface-based lifted condensation level (LCL, using T and q from the first model level), with $RH_{crit}=0.7$ and $p=2$. We take the maximum of these two calculations for the unstable case to ensure a smooth transition (i.e. no rapid changes in fractional cloud cover) from the stable to unstable regimes, and to acknowledge the possibility of convective or stratiform clouds.

2.6 Downward radiation

The model includes a simple radiation package which gives the total

downward radiation, a combination of incoming solar (shortwave) plus downward atmospheric (longwave) radiation (Ek and Mahrt, 1989).

The equation for net incoming solar radiation reaching the ground is then

$$S_n \downarrow = [1 - (1 - t)CLC^m] (1 - \alpha) S \downarrow \quad (39)$$

where $S_n \downarrow$ is the net incoming solar radiation, t a fraction dependent on the solar radiation transmitted through the clouds (currently 0.3 in the model), CLC is the fractional cloud, m is an empirically-derived coefficient (1.0 in the model), α is the surface albedo, and $S \downarrow$ is the clear sky solar radiation adjusted for solar elevation. When $m = 1$, t is the actual fraction of solar radiation transmitted through the clouds.

The expression for atmospheric radiation is (Ek and Mahrt, 1989),

$$L \downarrow = \epsilon \sigma T_{ref}^4 + c_2 CLC \quad (40)$$

where $L \downarrow$ is the noncloud atmospheric radiation; ϵ is the emissivity of the atmosphere, a function of the temperature and moisture at the reference level in the model (currently 200 m); T_{ref} is the fractional cloud cover; and c_2 is an empirically-derived constant equal to 60 W m^{-2} .

CHAPTER 3

METHODOLOGY

This chapter describes the data source used during this study, the antecedent retention index that developed for input to the model and describes the computer experimental runs that were compared in the results section

3.1 Data Source

The primary data source was taken from the Cooperative Huntsville Meteorological Experiment (COHMEX). This experiment took place from 1 June 1986 to 31 July 1986. The purpose of this experiment was to study the formation and interaction of thunderstorms. The south-central Tennessee - northern Alabama area is where the investigation took place (figure 1).

This work examined three days during the COHMEX experiment; 9 June, 17 June, and 16 July. Atmospheric soundings from Nashville, Tennessee (BNA) and Redstone Arsenal, Alabama (RSA) were used for the model runs. The Nashville soundings were taken from the National Weather Service data at 1200 GMT and 0000 GMT, and from COHMEX data tapes at other non-standard times. The Redstone Arsenal Soundings were released at

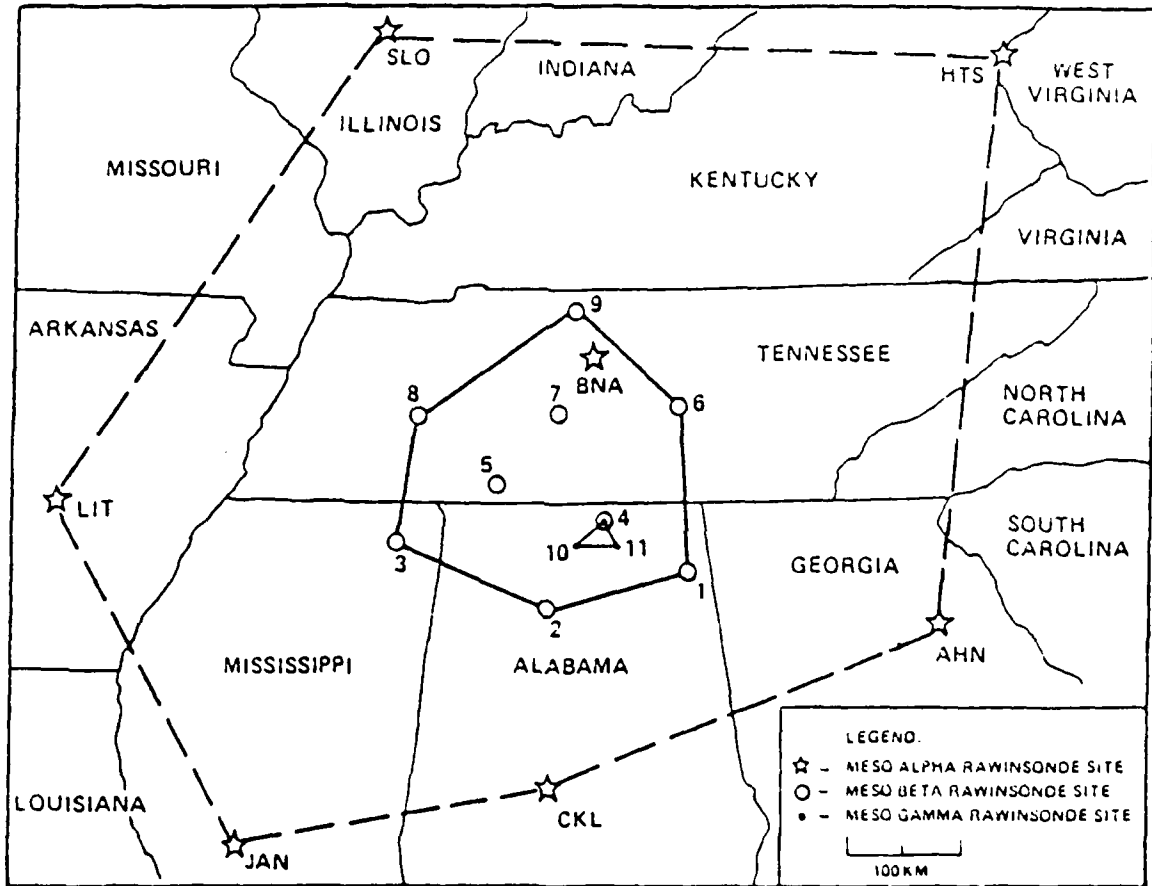


Fig. 1. The COHMEX rawinsonde network (solid lines). Nashville, Tennessee is located at BNA; Redstone Arsenal, Alabama is located at number 11.

1200 GMT and 1800 GMT. The 1200 GMT sounding was deployed to issue a forecast, while the 1800 GMT sounding was released to collect data for climatological purposes.

The Nashville and Redstone Arsenal sites were chosen for several reasons. The relative closeness of the sites permits us to examine two stations influenced by the same air mass that are both deploying soundings. The average spacing of radiosonde stations in the continental U.S. is 350 kilometers while the distance between Nashville and Redstone is 150 kilometers. This will permit an examination of subtle differences of the boundary layer over a small distance. Also, these two sites are far enough inland that a sea breeze should not effect the formation of convection.

Since this study is concerned with the formation of air-mass thunderstorms, the days tested were days where the forcing mechanisms mentioned in chapter one were considered to be weak. Three types of days were looked at: (1) when thunderstorm activity was over most of the COHMEX area (9 June), (2) when thunderstorm activity was widely scattered (16 July) and (3) when thunderstorms occurred over one portion of the COHMEX area, yet did not occur over another (17 June). This was done to test model temperature and dew-point temperature forecasts under a variety of conditions for future studies involving surface stability index.

3.2 Soil Moisture parameterization

Soil moisture was not measured during the COHMEX experiments. This

forced the author to investigate a method to estimate the soil moisture for input to the model.

Troen and Mahrt (1986) found in the OSU1DPBL model the height of the planetary boundary layer is a nonlinear function based upon soil moisture. They state that this nonlinear dependence of boundary layer growth rate on water availability is due to the reduction of potential evaporation associated with increased relative humidity of the boundary layer (figure 2). This shows how critical the soil moisture is to determining the boundary layer calculations in the model. The question is how can we find a simple, yet accurate determination of soil moisture that will yield results we can be confident in?

The method used for computing soil moisture in this study is the antecedent retention index (ARI) developed by Saxton and Lenz (1967). The soil model used in this work consists of two soil layers extending to a vertical depth of one meter. The top soil layer is 5 centimeters thick, while the bottom soil layer is 95 centimeters thick. Therefore, the top soil layer is subject to more of the daily fluctuation of soil moisture due to evaporation as well as precipitation. The top soil layer daily ARI is determined by the equation

$$ARI_i = ARI_{i-1} + R_{i-1} - PET \quad (41)$$

where i is the julian day, R is the precipitation in inches and PET is the potential evapotranspiration equal to 0.15 inches (Shultz, 1973). The PET is also a function of soil moisture. In our case the PET is equal to 0.15 until the ARI goes below 0.5. The PET then decreases linearly to zero as the ARI decreases to zero.

The value of the retention, R_{i-1} , is equal to the precipitation that falls the

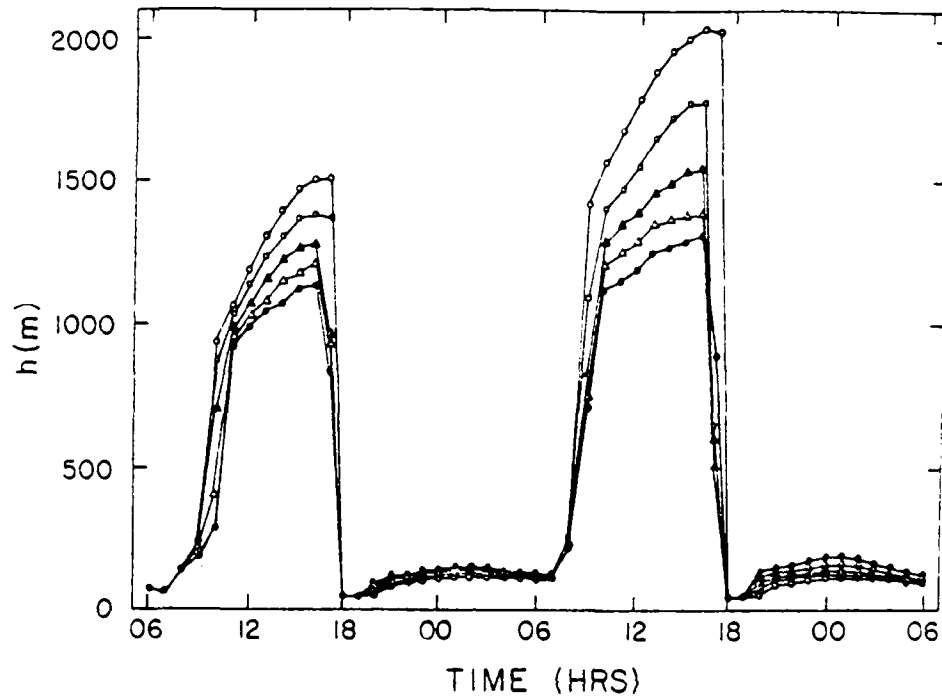


Fig. 2. The boundary-layer depth as a function of local standard time for water availability $b \equiv$ surface evaporation/potential evaporation = 0 (open circles), 0.25 (open squares), 0.50 (solid triangles), 0.75 (open triangles), and 1 (solid circles). (From Troen and Mahrt, 1986).

previous day. Therefore all the precipitation that falls is assumed to be retained by the soil and runoff is not considered unless the soil becomes saturated. This assumption will probably lead to an overestimation of soil moisture in cases of heavy precipitation, particularly when the precipitation falls during a short period of time.

Changes in the soil moisture of the lower soil level are going to be slower than the top soil layer. Depletion of soil moisture in the bottom soil layer is mostly due to gravitational flow through the bottom of the soil layer. The lower layer soil moisture is determined by the formula

$$ARI_i = (ARI_{i-1} + R_{i-1}) X \quad (42)$$

where X is the soil depletion index equal to 0.92 (Shultz, 1973). R_{i-1} is equal to precipitation from the previous day.

The maximum value of ARI is equal to 1.0. When this occurs, the field capacity of the soil has been reached, i.e., the soil is saturated. If the ARI became greater than 1.0 during the calculations, this excess moisture was considered to be runoff. By setting the maximum value of ARI equal to 1.0, the saturation of both soil layers occurs when 2.54 centimeters is available. Considering that the lower soil layer is 95 centimeters thick, this may also be a large source of error in these calculations.

The variable for soil moisture in the input file is called WSOIL. WSOIL is a volumetric soil water content. For the model runs in this work, the maximum volume of soil moisture is 40% or 0.4 of the soil. It is necessary to change the values of ARI for input into the model as WSOIL. This is done by simply multiplying the ARI by 0.4.

ARI_0 , the initial antecedent retention index, is the most critical variable in determining a daily ARI. The initial date for the calculation of ARI is 29 May 1986. For both BNA and RSA the, ARI_0 is equal to 1.0, the maximum value for ARI. Rainfall rates resulting in an ARI greater than 1.0 are considered to be runoff. The ARI_0 are the result of 2.26 inches of rain for 24 May to 28 May 1986 for BNA and 3.09 inches of rain at RSA during the same period. A complete listing of the variable names for the control file is available in Ek and Mahrt (1989). Table 1 shows the computed values of WSOIL used during this work (next page). The benefit of the three days that were chosen for this work is the ability to examine cases where the soil moisture is highly variable and determine how sensitive the model output is to soil moisture. The ARI values for BNA and RSA during the entire COHMEX period are shown in figure 3.

Figure 3 shows that the top soil layer (ARI 1) does not fall below 0.3 for BNA and RSA. This was done to prevent the soil moisture in this layer from falling below the input value for the wilting point. If, during the model run the value for soil moisture were to fall below the wilting point, evapotranspiration would stop. This would lead to a decrease in the latent heat flux and thereby lead to excessive heating and drying of the surface layer and decrease the accuracy of the T and T_d forecast. In future work, and in an operational environment, ARI would be coupled to the model-calculated potential evapotranspiration.

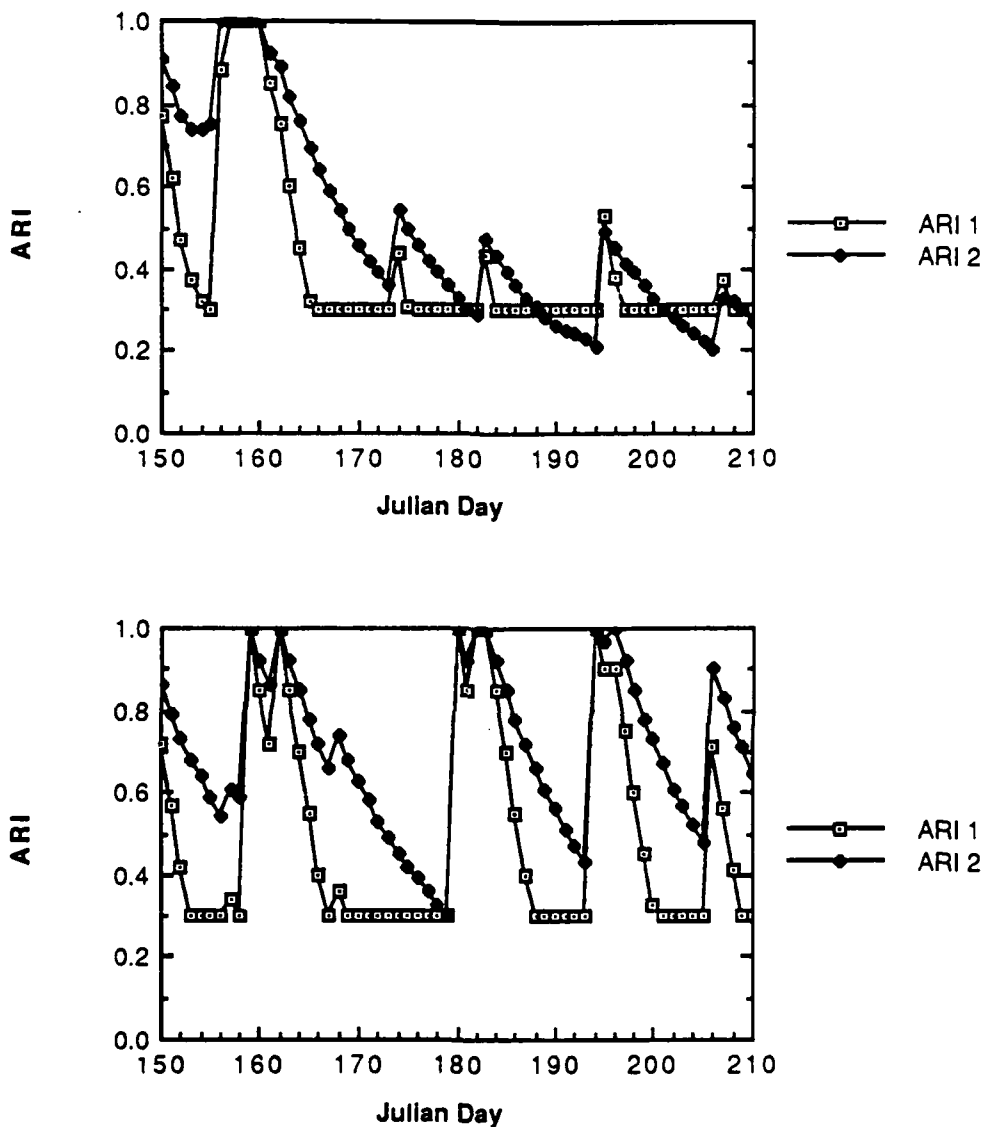


Fig. 3. Antecedent Retention Index values for Nashville, Tennessee (top) and Redstone Arsenal, Alabama. ARI 1 is the Antecedent Retention Index for the top soil layer (5 centimeters thick), ARI 2 is the Antecedent Retention Index for the lower soil layer (95 centimeters thick). ARI = 1.0 indicates a saturated soil; ARI = 0.0 indicates no soil moisture. June 1 is Julian day 152, and July 29 is Julian day 210.

Table 1. The computed values of WSOIL for Nashville, Tennessee and Redstone Arsenal for the three days examined during this work. A WSOIL value of 0.40 indicates a completely saturated soil. WSOIL(1) is 5 centimeters in depth and WSOIL(2) IS 1 meter in depth.

		RSA	BNA
9 June	WSOIL(1)	0.34	0.40
	WSOIL(2)	0.37	0.40
17 June	WSOIL(1)	0.14	0.11
	WSOIL(2)	0.30	0.22
16 July	WSOIL(1)	0.30	0.12
	WSOIL(2)	0.37	0.16

3.3 Determination of Shelter Temperature

The results of this work are centered upon the temperature and dew-point temperature forecasting capabilities of this model. As such, it is important to understand how the model computes these values. A temperature and dew-point temperature profile is forecast every hour. The first model level above the surface for these profiles is 20 meters. The model interpolates the value for two meter (shelter) T and T_d using the method of Holtslag and de Bruin (1988), where in the atmospheric surface layer a temperature difference $T_2 - T_1$ between two levels z_2 and z_1 is given by

$$T_2 - T_1 = \frac{\theta_*}{k} \left[\ln \left(\frac{z_2}{z_1} \right) - \psi_H \left(\frac{z_2}{L} \right) + \psi_H \left(\frac{z_1}{L} \right) \right] - \Gamma_d (z_2 - z_1) \quad (43)$$

where k is the von Kármán constant, Γ_d the dry adiabatic lapse rate and ψ_H is the stability function for heat, which is a function of z and the Monin-Obukhov length scale L , defined by

$$L = \frac{u_*^2}{k \frac{g}{T} \theta_*} \quad (44)$$

Here g is the acceleration of gravity and T air temperature. Furthermore, θ_* is the turbulent temperature scale, which follows from

$$H = -\rho C_p u_* \theta_* \quad (45)$$

where ρC_p is the volumetric heat capacity of the air at constant pressure and u_* is the friction velocity. Once the temperature difference is known, it is quite simple to find the two meter temperature and dew-point temperature.

3.4 The Experimental Procedure

The computer runs for this experiment examined three days during COHMEX. 9 June and 16 July where a high pressure system dominated the COHMEX area and 17 June which had a weak cold front pass through the region.

The Nashville and Redstone soundings for these days had four separate computer runs performed to examine what influence various parameters in the input file would have on the temperature and dew-point temperature forecasts of the model. The vertical velocity profile for each of the four computer runs is equal to zero; hence the effects of subsidence or rising motion upon the growth

and development of the planetary boundary layer are not taken into account. Procedures for including estimates of ω for future work are discussed in chapter five. The first of the experiments is known as the original run (experiment A).

The original run consists of a soil moisture of 50 per cent for both soil layers. This is essentially a "first-guess" since soil moisture readings were not taken during COHMEX. The soil type used during the original run is sandy clay loam - which is the default soil type in the model input file. A value of 0.12 is set for the wilting point, TWILT; that is when the value of WSOIL becomes less than 0.12 during the model run, evapotranspiration will stop.

The second experiment is known as ARI (experiment B). The difference between this experiment and the original run is that the derived values for WSOIL(1) and WSOIL(2) are used in the input file. This test is done to determine if the ARI program will result in a better estimate of soil moisture than by simply guessing and therefore give a better forecast for shelter height temperature, dew-point temperature, and PBL height. The soil type and wilting point are unchanged.

The third experiment is called NS (experiment C). According to Bennett (1921) clay loam is the dominant soil type in the COHMEX region. Bennett also states that the difference between clay loam and sandy clay loam (the default soil type used in experiment A and B) is while both are between 20 to 30 per cent clay and less than 50 percent silt; clay loam has slightly less than 20 per cent of its composition made up of sand, while sandy clay loam has a composition of slightly more than 20 per cent sand. Clay soil is defined as being greater than 30 per cent clay, less than 45 per cent silt and having no

sand (Bennett, 1921). In experiment C, the soil type is changed from sandy clay loam to clay. This is done in the hope that the slower rate of depletion of soil moisture of the clay soil will prevent excess sensible heating and give a better forecast. WSOIL is maintained at ARI values and the wilting point is still 0.12.

The fourth and final run is known as WILT (experiment D). The wilting point of the clay soil is decreased to 0.04 (about 10 per cent of its saturation value). This is done to determine the influence the wilting point has on model output, particularly for periods of low soil moisture by allowing for the continuation of evapotranspiration and thereby increasing the latent heat flux. The WSOIL values are from experiment B.

Model default values for all the experiments can be found in appendix A

Table 2. Experiments run vs. the variables that are changed.

EXPERIMENT	WSOIL	SOIL TYPE	WILTING POINT
A	0.2, 0.2	SANDY CLAY LOAM	0.12
B	ARI VALUES	SANDY CLAY LOAM	0.12
C	ARI VALUES	CLAY	0.12
D	ARI VALUES	CLAY	0.04

CHAPTER 4

RESULTS

The results are divided into four major sections. The first, analyzes the square of the linear correlation coefficient, R^2 , which can be interpreted as per cent of variance explained, between observed and forecast temperature and dew-point temperature. The second section examines significant changes in the planetary boundary layer height to see if these changes lead to better forecasts of temperature and dew-point temperature. The third section examines the 17 June COHMEX case and the ability of the model to handle a frontal situation. The fourth and final section investigates the model cloud cover and its effect on T and T_d forecasting.

4.1 Statistical Temperature Comparisons

Scatter diagrams were plotted for all experimental runs of temperature and dew-point temperature versus the actual temperature and dew-point. The square of the linear correlation coefficient, R^2 was computed for each case (48 calculations) (table 3). R^2 can have values of zero to unity and according to Panofsky and Brier (1968) R^2 measures the percentage of the total variance

Table 3. R^2 values for Redstone Arsenal, Alabama and Nashville, Tennessee on 9 June 1986, 17 June 1986 and 16 July 1986. \ \equiv negatively correlated, A \equiv original run, B \equiv new WSOIL, C \equiv NS, D \equiv WILT

	RSA		BNA		
	T	Td	T	Td	
9 June	0.948	0.005	0.621	0.587\	A
	0.976	0.634\	0.668	0.571	B
	0.965	0.562\	0.672	0.594	C
	0.964	0.556\	0.677	0.594	D
17 June	0.787	0.691	0.783	0.012	A
	0.812	0.082	0.874	0.032	B
	0.801	0.130	0.800	0.012	C
	0.809	0.345	0.801	0.017	D
16 July	0.677	0.027	0.978	0.004	A
	0.633	0.256	0.971	0.007	B
	0.694	0.549	0.982	0.009	C
	0.696	0.530	0.982	0.005	D

The R^2 scores can be summarized as follows:

- (1) R^2 improved 4 of 6 times for T and T_d when the computed values of WSOIL are entered.
- (2) R^2 improved 6 of 6 times for T and improved 3 of 6 times for T_d for A vs. C.
- (3) R^2 improved 6 of 6 times for T and 4 of 6 times for T_d for A vs. D.
- (4) R^2 improved 3 of 6 times for T and 4 of 6 times for T_d for B vs. C.
- (5) R^2 improved 3 of 6 times for T and 3 of 6 times for T_d for B vs. D.
- (6) R^2 improved 1 of 6 times for T and 2 of 6 times for T_d for C vs. D.

accounted for by variation by two elements and is an indication of the accuracy of a forecast.

These results show that the best results occur when WSOIL, soil type and TWILT are all changed. It also shows that the new values for soil moisture that were computed from the ARI program do have a significant difference and are a step in the right direction. Also shown is that changing the soil type regardless of the wilting point does improve the forecast, while changing only the wilting point of the soil does not significantly improve the R^2 score of T or T_d . The reader may note some of the R^2 scores are negatively correlated. These scores will be examined in detail in section 4.2.

These results may be misleading due to the small sample size. Another thing to note is while the R^2 values do show improvement, the actual magnitude of change is small. The average change in R^2 scores for temperature is 0.024. However, the range of R^2 scores for dew-point temperature is much greater and it is the dew-point temperature forecast that our attention will be focused on.

4.2 PBL Height Comparisons

Among the most striking items in the model output is the change in the diagnosed height of the planetary boundary layer (PBL) with the change in soil moisture as a result of changes in the surface energy balance. Corresponding to the changes in PBL height are changes in the Bowen ratio. The Bowen ratio

is simply the ratio of sensible heat flux to the latent heat flux. Therefore, if the Bowen ratio is greater than unity, sensible heat flux is larger than latent heat flux. This may be found over surfaces where water is limited (Oke, 1978). The opposite is true when the Bowen ratio is less than one. The next section will discuss if a significant change in PBL height and Bowen ratio lead to an improvement in dew-point forecasting. In particular, three cases will be examined, 9 June at Redstone, 9 June at Nashville and 16 July at Redstone. The 16 July Nashville will also be presented. Although this case had little change in the PBL height forecast between the four experiments, large fluctuations did exist between the Bowen ratios.

4.1.2 9 June Synoptic Overview. A stationary front was located just to the north of the COHMEX region with little movement present over the next 24 hours (figure 4). A 1025 millibar surface high pressure system was centered over the Great Lakes region with southerly flow of four to eight knots over the southeastern United States. At 50 kPa a broad pressure ridge dominated the eastern third of the U.S. with southwesterly winds at 10 to 20 knots found over the southeast (fig 5).

4.1.2a 9 June - Redstone. Examining the changes in the forecast height of the planetary boundary layer for Redstone on June 9; the PBL reaches a height of 2400 meters by 14 L during experiment A (fig 6). Once the increased soil moisture is introduced, the growth of the PBL is considerably slower and reaches a height of only 1300 meters for experiments B, C & D.

The Bowen ratio is four times larger during experiment A than the other three experiments; thus sensible heating dominates during experiment A (fig



Fig. 4. NMC surface analysis for 1200 GMT 9 June 1986.

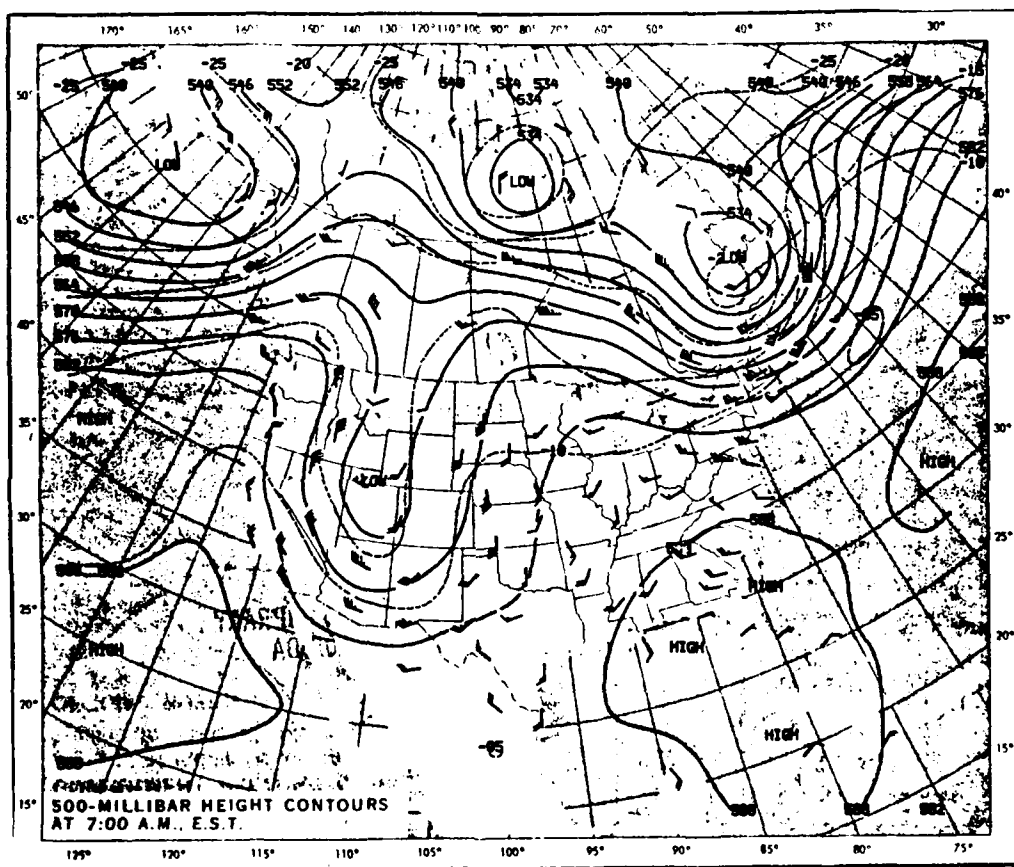


Fig. 5. NMC 50 kPa analysis for 1200 GMT 9 June 1986.

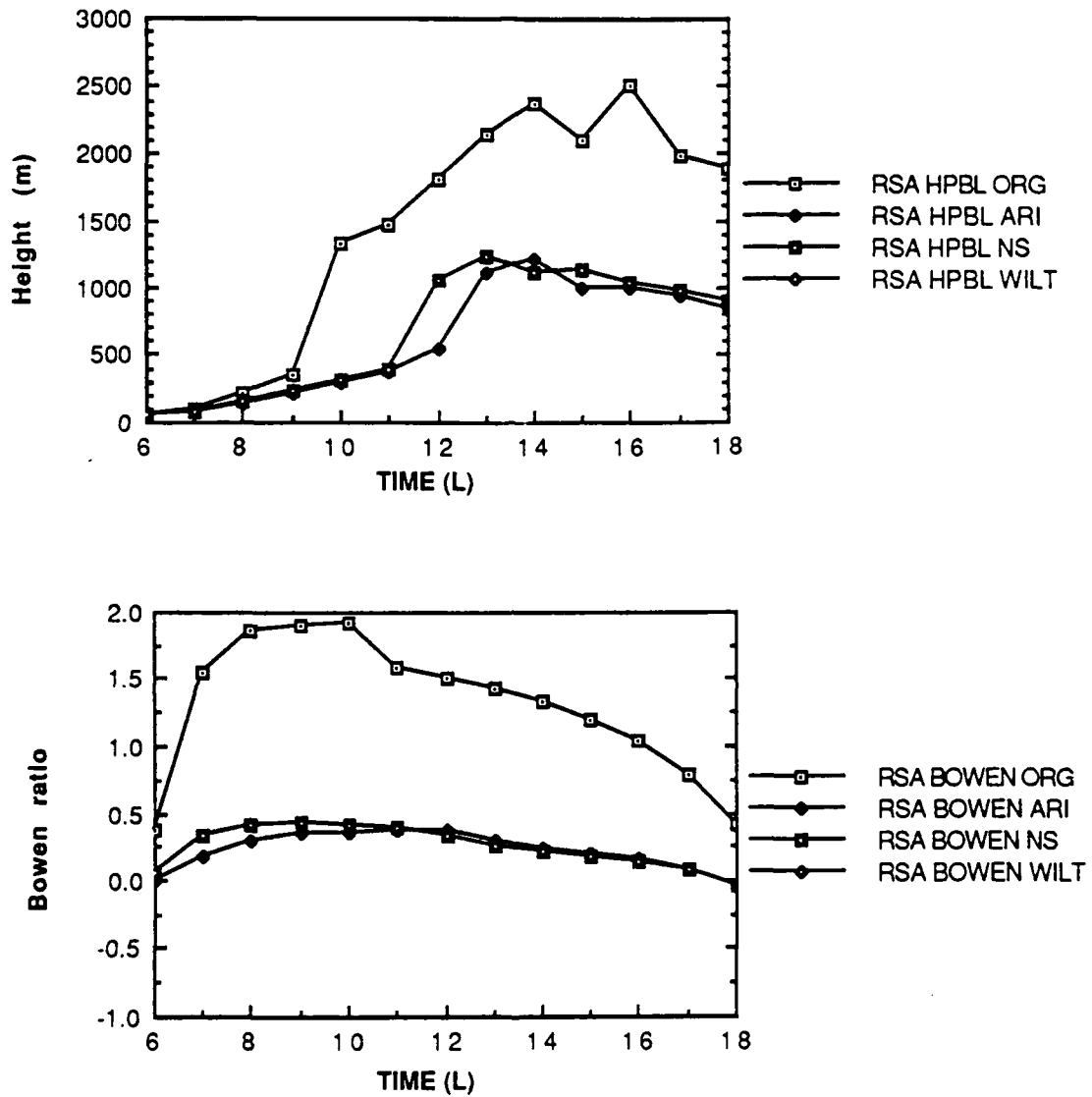


Fig. 6. The planetary boundary layer height in meters (top), and the Bowen ratio (bottom) for Redstone Arsenal, Alabama; 1200 GMT, 9 June 1986. ORG, experiment A; ARI, experiment B; NS, experiment C; WILT, experiment D.

6). When the new values for WSOIL are used, the Bowen ratio becomes a more modest 0.4 - agreeing more closely with the expected values for temperate forest and grasslands according to Oke (1978).

Does this decrease in PBL height and the Bowen ratio result in better R^2 values? For temperature the answer is yes, but very slightly. In the original run R^2 is 0.948, while the increase in soil moisture produces an R^2 of 0.978, or an increase of 2.8 per cent. Both values indicate extremely good performance.

R^2 for dew-point temperature is a poor 0.005 for the original run and is a negatively correlated 0.634 when the soil moisture is increased. The introduction of clay soil and lowering the wilting point don't improve the R^2 scores, as they are a negatively correlated 0.556 and 0.562 respectively.

The explanation as to why the temperature forecasts did so well in comparison to the dew-point temperature forecasts can be seen in the time series plots (fig 7). The large amount of sensible heating leads to a rapid increase in T and a decrease in T_d . The actual dew-point temperature drops from 72° F to 64° F by 9 L and fluctuates between 64° F and 66° F during the remainder of the day. Since the observed trend is downward and the forecast trend is upward, a negative correlation results.

The introduction of ARI soil moisture produces a better temperature forecast, but the model's response to the abundance of soil moisture is to keep T_d too high as the latent heat flux increases by 100 W/m^2 and the sensible heat flux decreases by 150 W/m^2 at 13 L (fig 8). An average spread of 14 degrees between the forecast dew-point and the actual dew-point results. Therefore in this case a sharp decrease in PBL height and Bowen ratio does not yield a

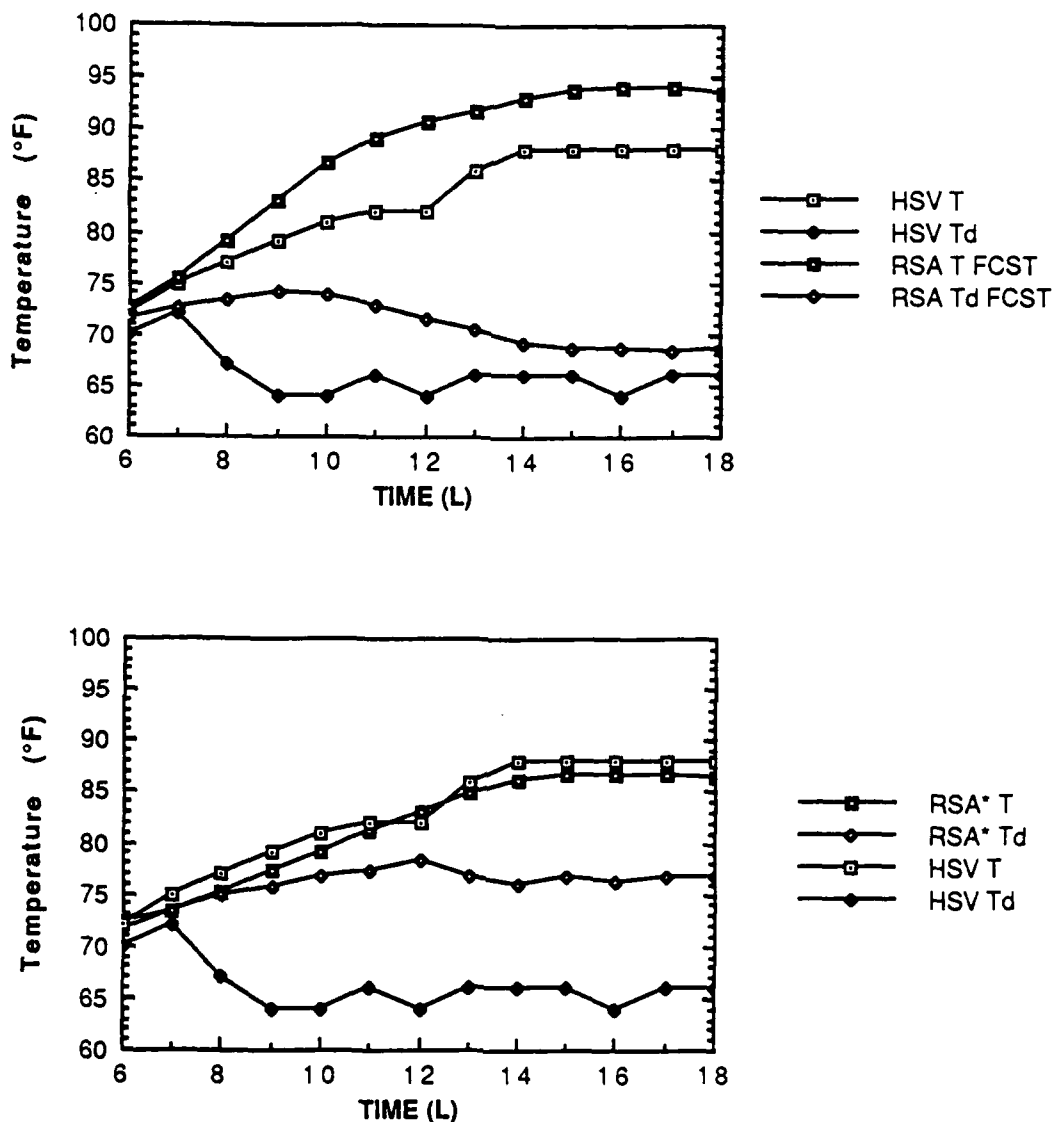


Fig. 7. Temperature and dew-point temperature traces with forecast two meter temperature and dew-point temperature trace for Redstone Arsenal, Alabama, 9 June 1986. Top - experiment A, bottom - experiment B. HSV T - Huntsville temperature, HSV Td - Huntsville dew-point temperature. RSA T FCST - Temperature forecast from experiment A, RSA Td FCST - dew-point temperature forecast from experiment A. RSA* T - temperature forecast from experiment B, RSA* Td - dew-point temperature forecast from experiment B.

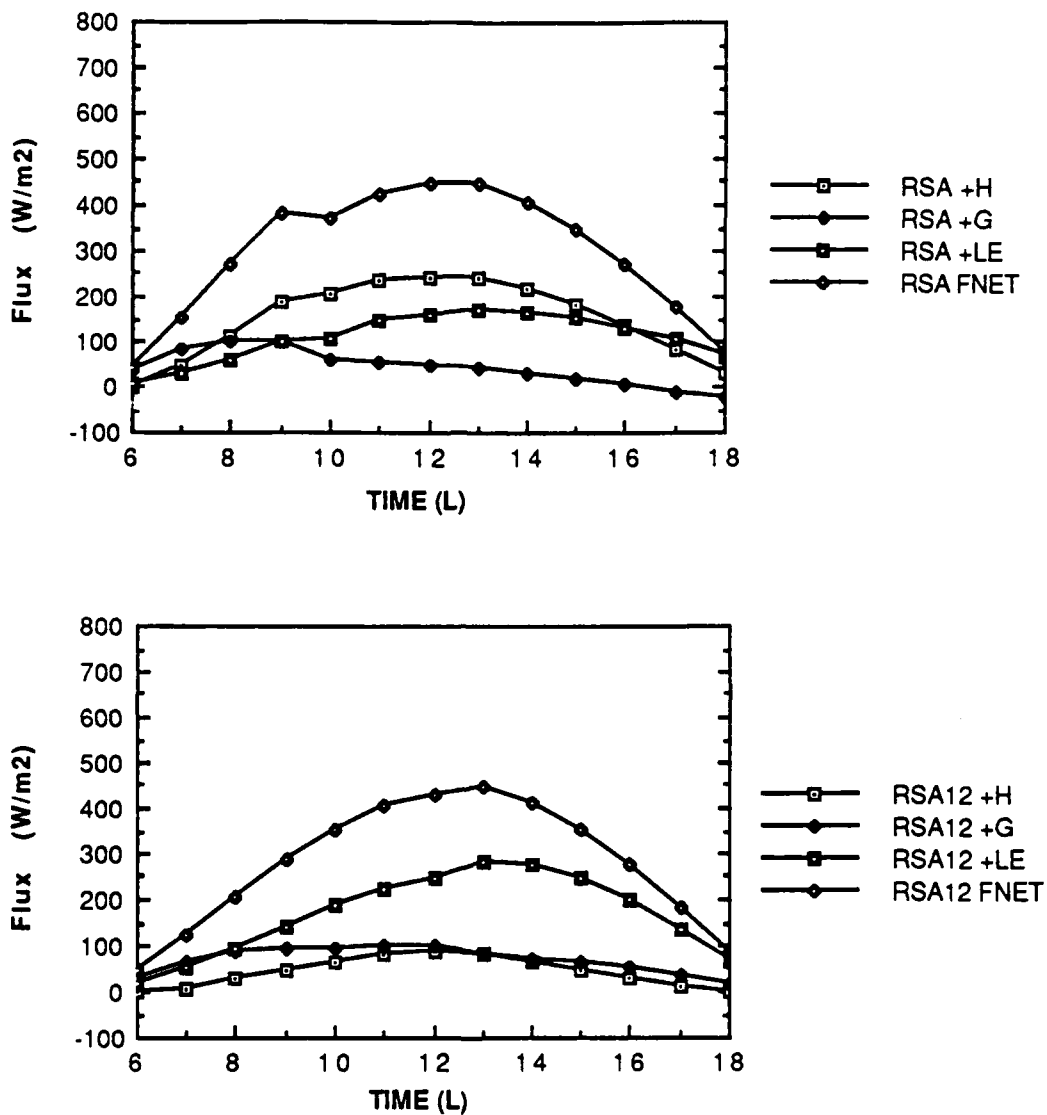


Fig. 8. Surface energy balance for Redstone Arsenal, Alabama 9 June 1986. Top - experiment A, bottom - experiment B. +H, Sensible heat flux (positive upward, $W m^{-2}$); +G, soil heat flux (positive downward, $W m^{-2}$); +LE, latent heat flux (positive upward, $W m^{-2}$); FNET, net radiation (positive upward, $W m^{-2}$).

significantly better dew-point temperature forecast.

4.1.2b 9 June - Nashville. This case also shows the influence of increased soil moisture. The PBL height for the original run reaches 1800 meters while the PBL height never exceeds 1100 meters for experiments B, C & D (fig 9). The Bowen ratio also shows a significant difference. While the Bowen ratio peaks at about 2.0 during the experiment A, it never is larger than 0.3 for the other experiments (fig 9).

The R^2 value for the original run for temperature is 0.621, while the ARI R^2 improves to 0.688. The clay soil and the lower wilting point cases offer no breakthroughs as the values of R^2 are 0.672 and 0.677 respectively.

The dew-point temperature R^2 do yield impressive results in this case. The dew-point R^2 for the original run is a negatively correlated 0.587. The increased soil moisture improves the R^2 score to a positively correlated 0.571. Changing the soil to clay and lowering the wilting point both result in a slight further improvement of R^2 to 0.594.

The role of soil moisture can also be seen by examining the T and T_d time series. Where the lack of soil moisture results in too much drying (fig 10), the higher soil moisture content results in a dew-point temperature trace that closely matches the actual dew-point trace (fig 10). If not for a sudden rise in the dew-point at 13-14 L the R^2 scores would probably be better. Therefore, in this case it appears that the soil moisture plays an important role in the surface energy balance and the T_d forecast and probably results in a more accurate forecast of PBL height.

4.2.2 16 July Synoptic Overview. The dominant feature on this day was

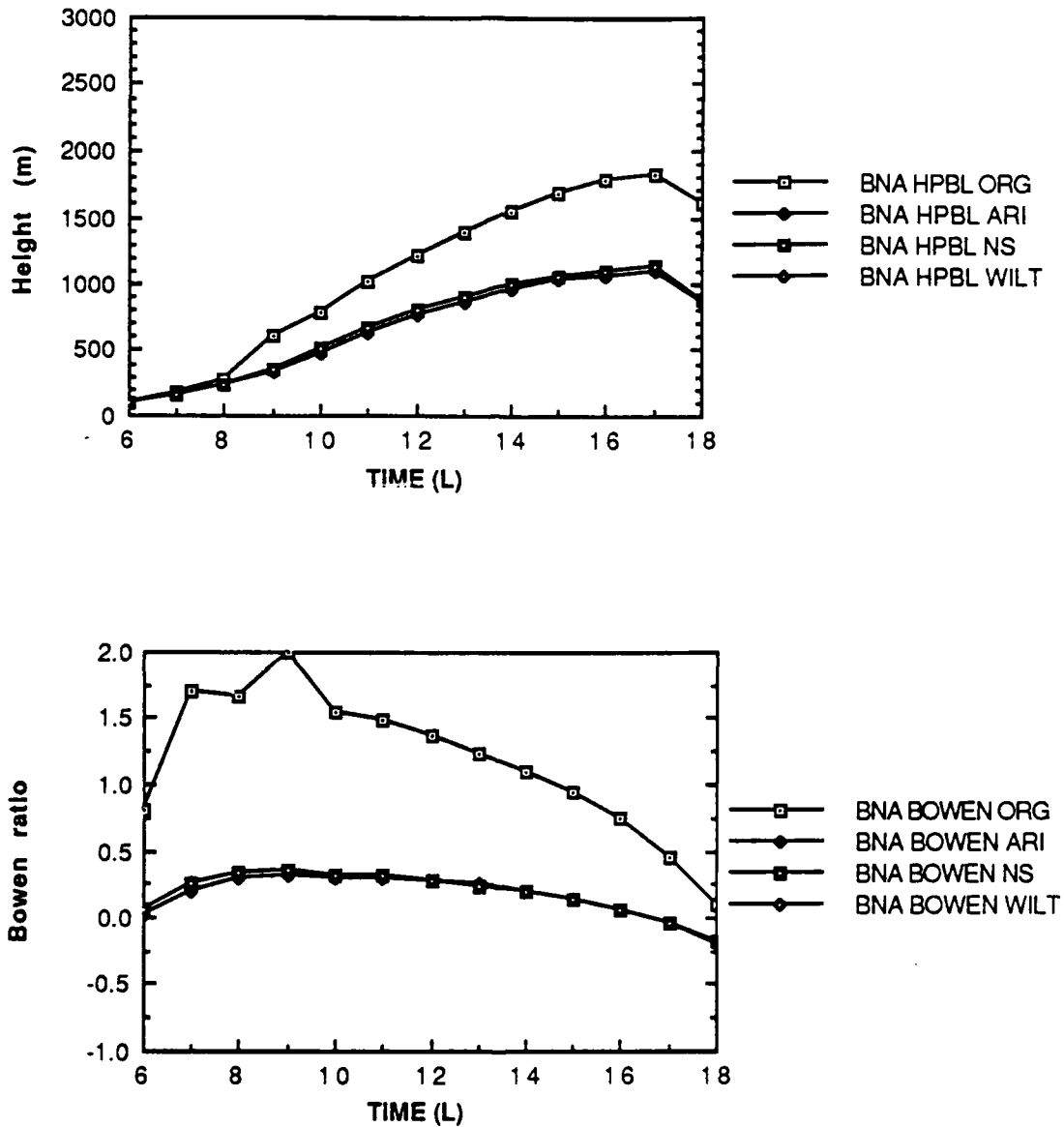


Fig. 9. The planetary boundary layer height in meters (top); and the Bowen ratio (bottom) for Nashville, Tennessee; 1200 GMT, 9 June 1986. ORG, experiment A; ARI, experiment B; NS, experiment C; WILT, experiment D.

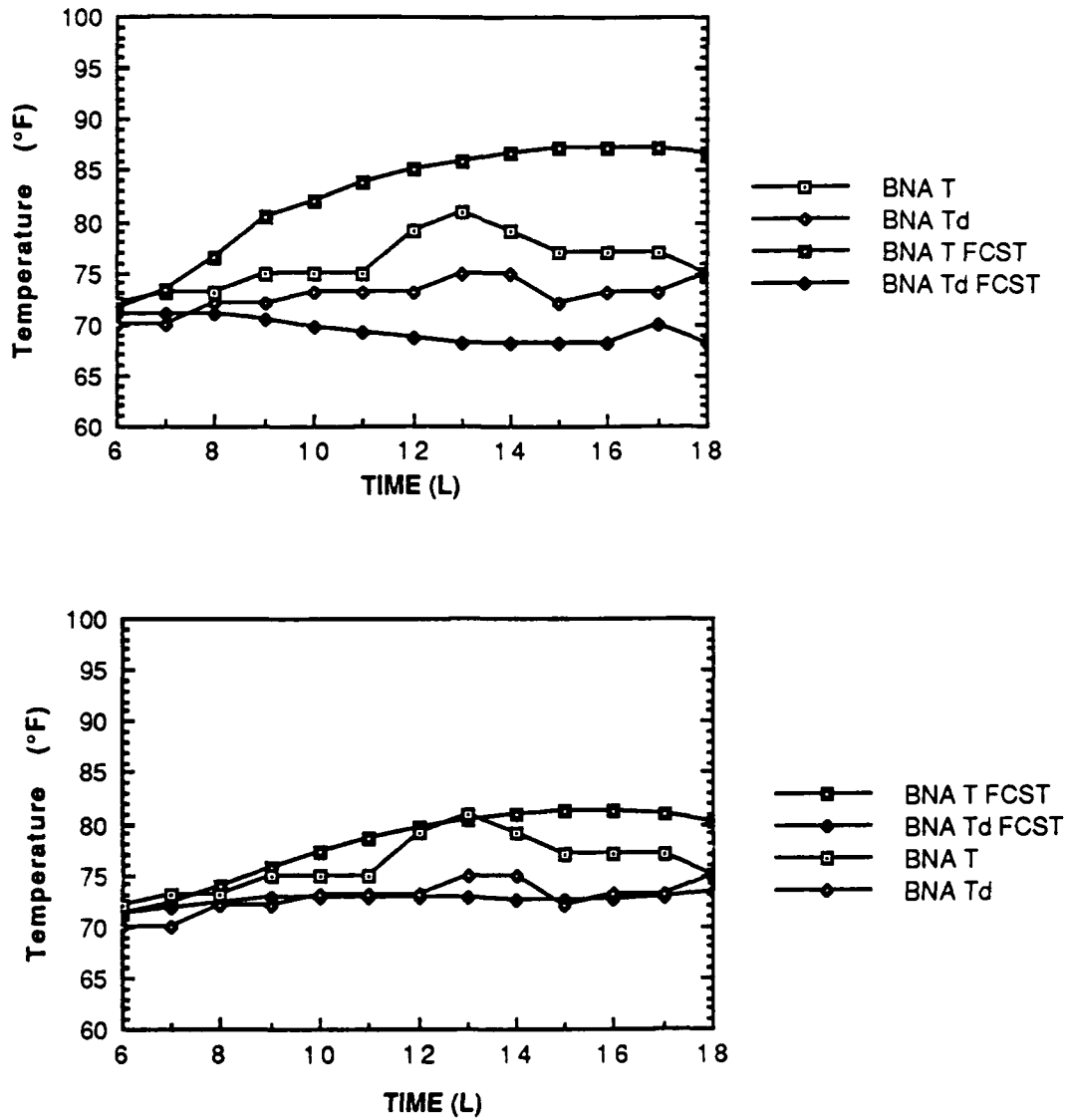


Fig. 10. Temperature and dew-point temperature traces with forecast two meter temperature and dew-point temperature traces for Nashville, Tennessee, 1200 GMT 9 June 1986. Top - experiment A, bottom - experiment B. BNA T - Nashville temperature trace, BNA Td - Nashville dew-point temperature trace. BNA T FCST - Nashville forecast temperature trace, BNA Td FCST - Nashville forecast dew-point temperature trace.

an extremely strong 50 kPa ridge that dominated the eastern half of the U.S. (fig 11). Winds at the surface in the COHMEX region were light and variable (fig 12), while at 50 kPa winds were easterly at 5 to 10 knots.

4.2.2a 16 July - Redstone. The height of the PBL for this case is slightly different from the other two cases. While the PBL height does drop sharply as WSOIL is increased, PBL height actually increases as soil type is changed to clay (fig 13). This trend also appears in the Bowen ratio curves, as the introduction of clay soil results in an increase in sensible heating and increases the Bowen ratio as well (fig 13).

The increase of soil moisture decreases the R^2 from 0.677 to 0.633 for temperature, while the clay soil run improves the R^2 to 0.696.

For T_d , the original run yields a poor R^2 value of 0.027. Experiment B increases the R^2 to 0.256 - which still does not show any skill in forecasting. However, the best R^2 for T_d results in the clay soil run as R^2 improves to 0.549 - a forecast indicating some skill.

However, the R^2 values in this case appear to be misleading. The T_d forecast trace in experiment A at one point crosses over the actual T_d trace (fig 14), while in experiment C, the forecast T_d trace is about 4° F warmer than the actual T_d trace on average. It appears as if the statistical calculations give an unfair advantage to experiment C. Therefore it is important that we not only restrict the evaluation of the forecasts to a single statistic, but to look at the actual data as well. The conclusion here is that the decrease in PBL height and Bowen ratio through increased soil moisture does not lead to a better T_d forecast.

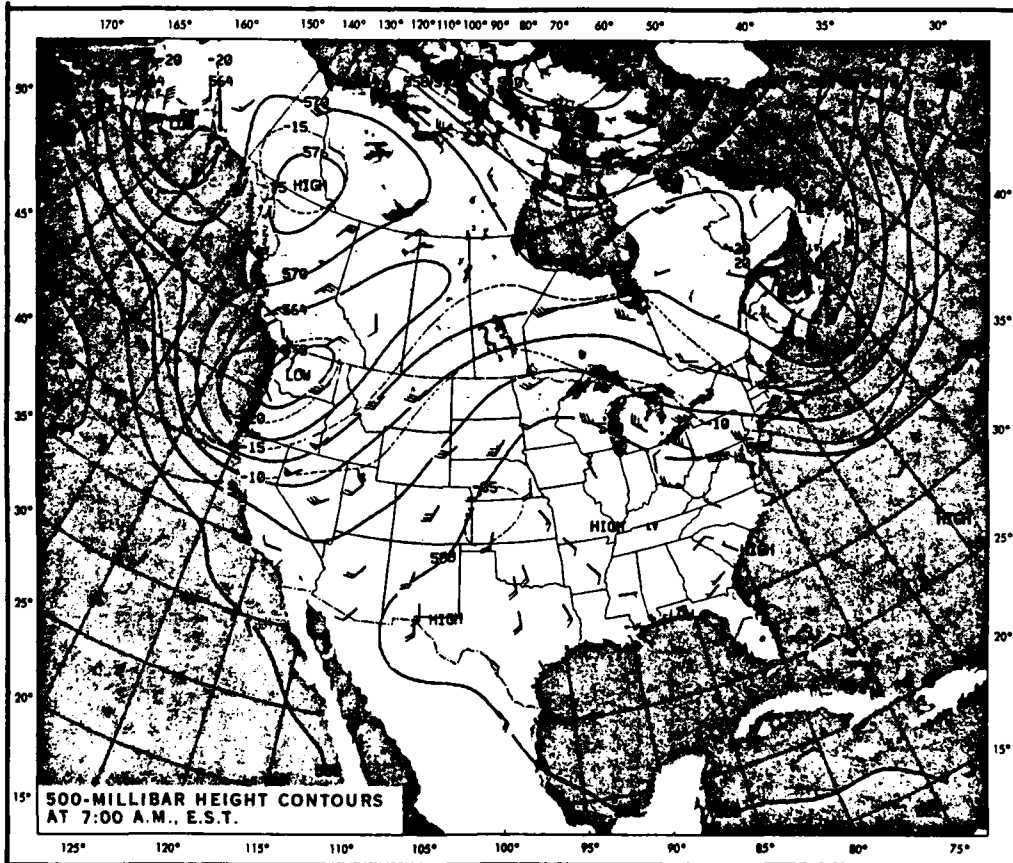


Fig. 11. NMC 50 kPa analysis for 1200 GMT 16 July 1986.

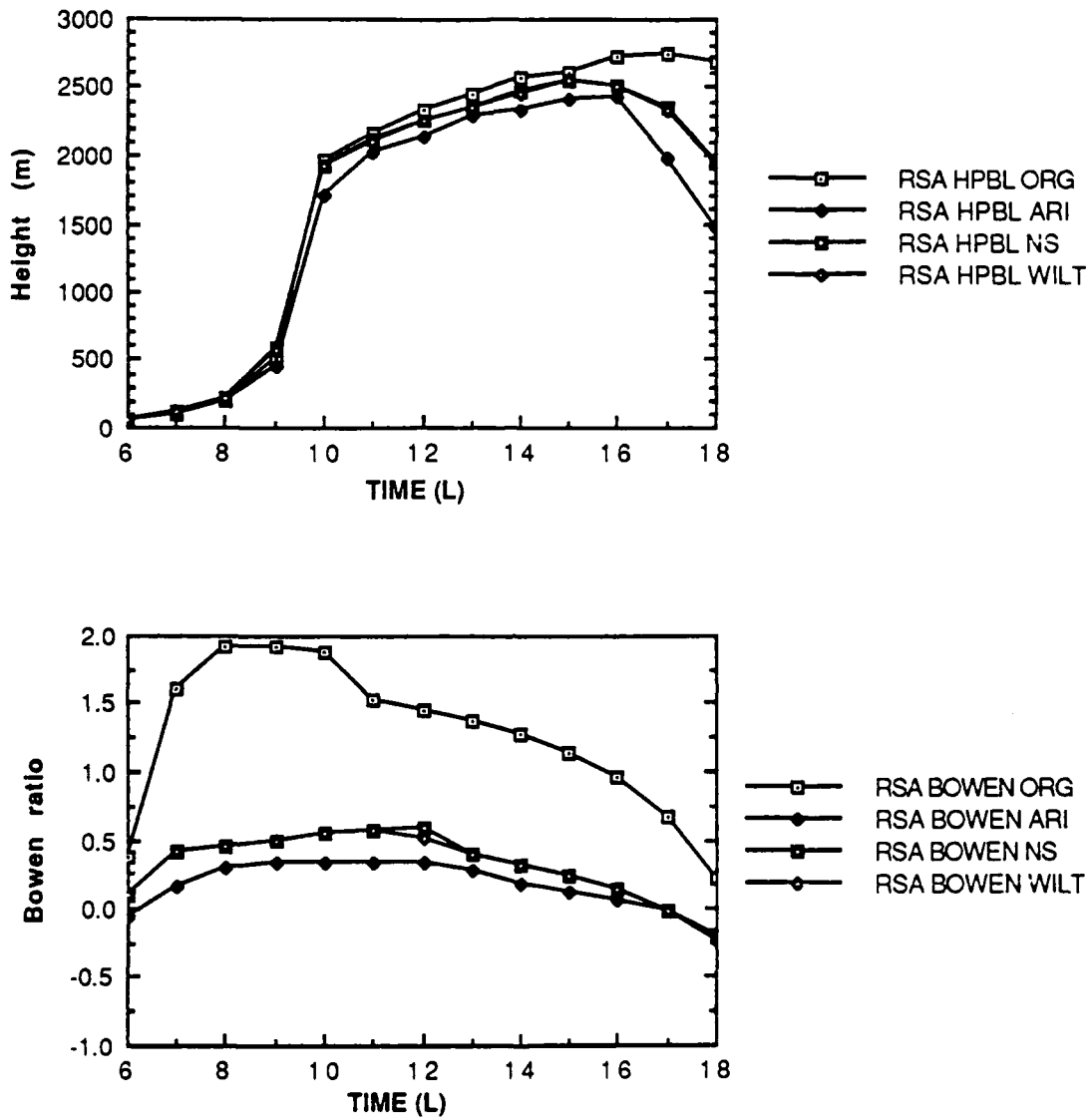


Fig. 13. The planetary boundary layer height in meters (top), and the Bowen ratio (bottom) for Redstone Arsenal, 1200 GMT, 16 July 1986. ORG, experiment A; ARI, experiment B; NS, experiment C; WILT, experiment D.

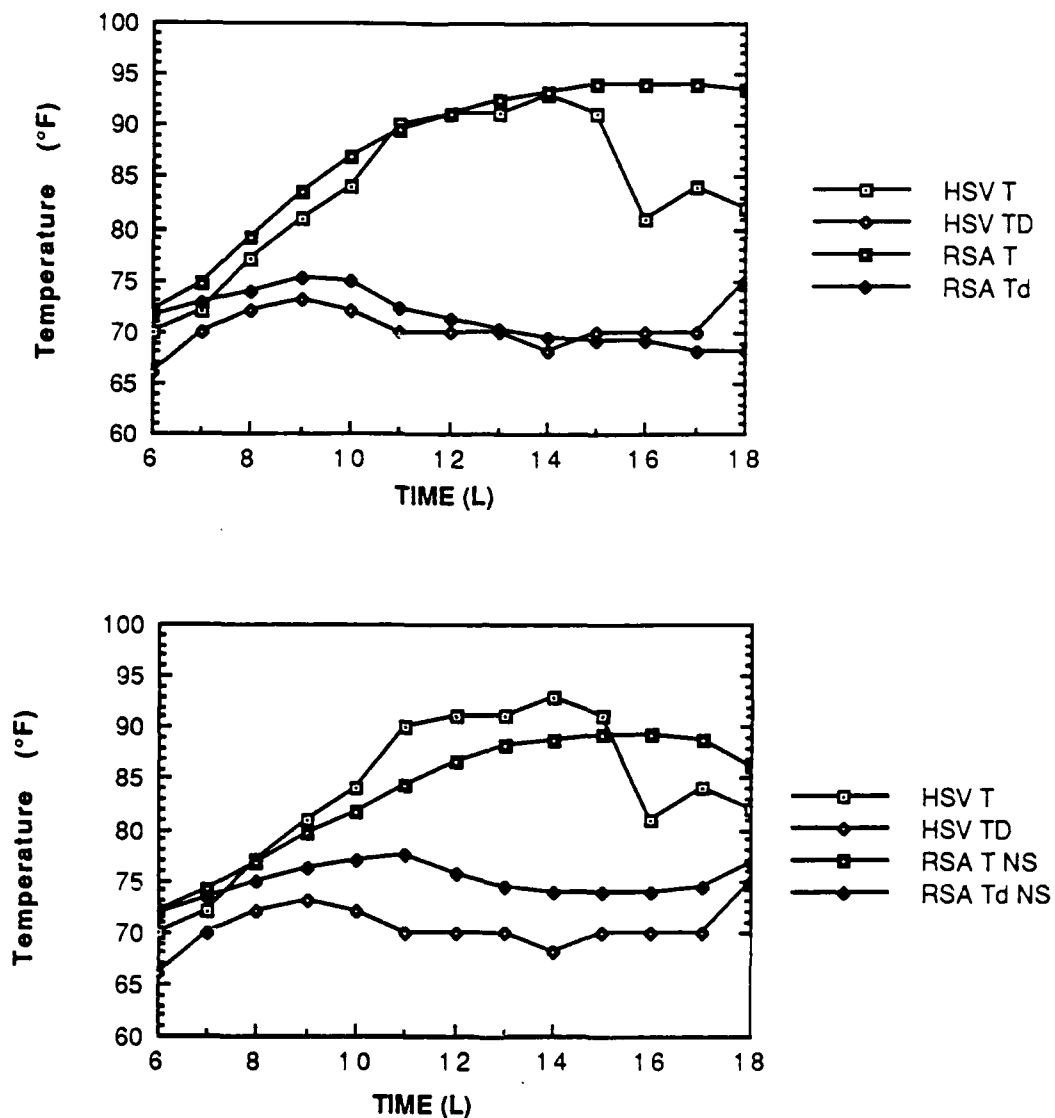


Fig. 14. Temperature and dew-point temperature traces with forecast two meter temperature and dew-point temperature traces for Redstone Arsenal, Alabama, 1200 GMT, 16 July 1986. Top - experiment A, bottom - experiment B. HSV T - Huntsville temperature trace, HSV Td - Huntsville dew-point temperature trace. RSA T - Redstone forecast temperature trace, RSA Td - Redstone forecast dew-point temperature trace. RSA T NS - Redstone forecast temperature trace, experiment C; RSA Td NS - Redstone forecast dew-point temperature trace, experiment C.

4.2.2b 16 July Nashville. While the first three cases presented show significant differences in planetary boundary layer height with the input of new values of soil moisture, the 16 July case at Nashville does not show these differences (figure 15).

The three weeks prior to 16 July at Nashville were very dry, as only 0.58 inches of rainfall were recorded. This led to the ARI program calculating values of 0.12 and 0.16 respectively for the top and bottom soil layer. Figure 15 shows very little change in forecast PBL height despite the variability between experiments. A 300 meter difference between experiment A and experiments B and C begins at 0900 local and perpetuates until 1700 local. Therefore by inspecting the PBL height, it would appear that the soil moisture has little impact on output.

However, when the Bowen ratios are examined, this is clearly not the case. Figure 15 shows the Bowen ratios for Nashville. The Bowen ratios are not in agreement with Oke's values (1978), and in experiments B and C are much greater than Oke's values of 0.4 to 0.8. This output was surprising; unlike the previous three cases, changes in the Bowen ratios did not correlate with changes in the planetary boundary layer height.

A closer examination of the Bowen ratios reveals several interesting model characteristics. Looking at experiment A vs. experiment B, what was expected to occur did happen as a decrease in soil moisture did lead to an increase in sensible heating and hence, to Bowen ratio. While changing the soil type in experiment C did not lead to any significant changes, reducing the wilting point in experiment D to 0.04 significantly changed the Bowen ratio.

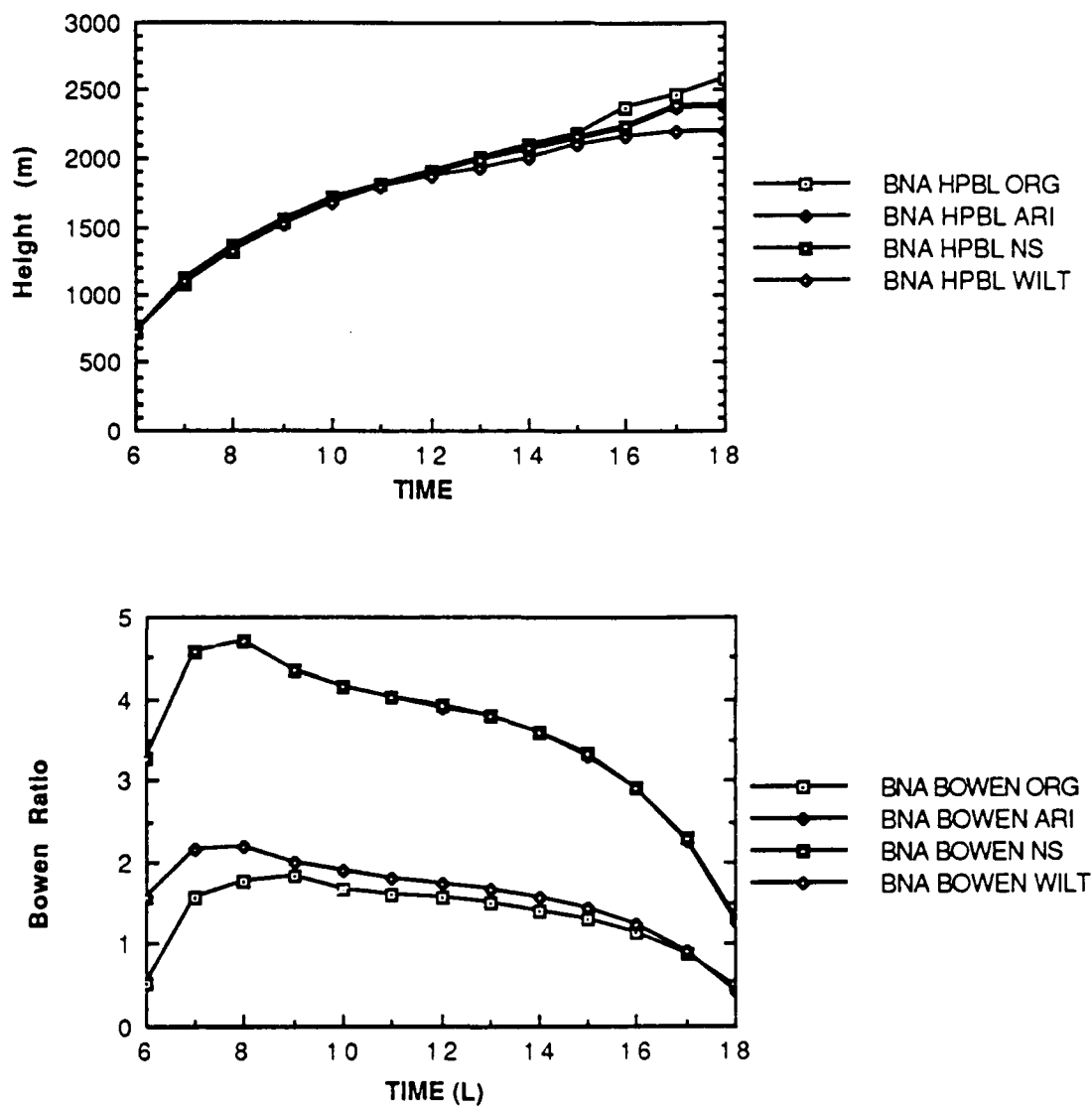


Fig. 15. Forecast PBL height (top) and Bowen ratio (bottom) for Nashville, Tennessee on 16 July 1986. ORG \equiv experiment A, ARI \equiv experiment B, NS \equiv experiment C and WILT \equiv experiment D.

Physically, this is what was expected as the initial value of WSOIL(1) was identical to the wilting point. By reducing the wilting point, evapotranspiration was allowed to continue for a longer time period of time, thereby increasing the latent heat flux and decreasing the Bowen ratio.

A look back at the R^2 values for this case reveals that despite the Bowen ratio fluctuations, the correlation coefficients followed the PBL height trends in that little difference occurred between R^2 scores. While the R^2 scores for T were excellent (between 0.971 and 0.982), the scores for T_d were quite poor (between 0.004 and 0.007). The explanation for the poor T_d scores can be seen in figure 16. While the actual dew-point temperature remains fairly constant at 72 °F, the forecast dew-point temperature drops down to 64 °F for experiments A and B.

Several physical explanations could be possible as to why the dew-point temperature was underforecast. The boundary layer could have grown into dryer air aloft. This dryer air may have been entrained into the boundary layer, thereby lowering the surface dew-point temperature during the mixing process. However, the possibility also exists that a mesoscale feature advecting moisture into central Tennessee could have overcompensated for any drying taking place and kept the dew-point temperature at 72° F. This points out the problem of using a one-dimensional model. Since advection during a short time period can be significant, an advection parameterization must be incorporated into the model if it is to be successfully used for air-mass thunderstorm forecasting.

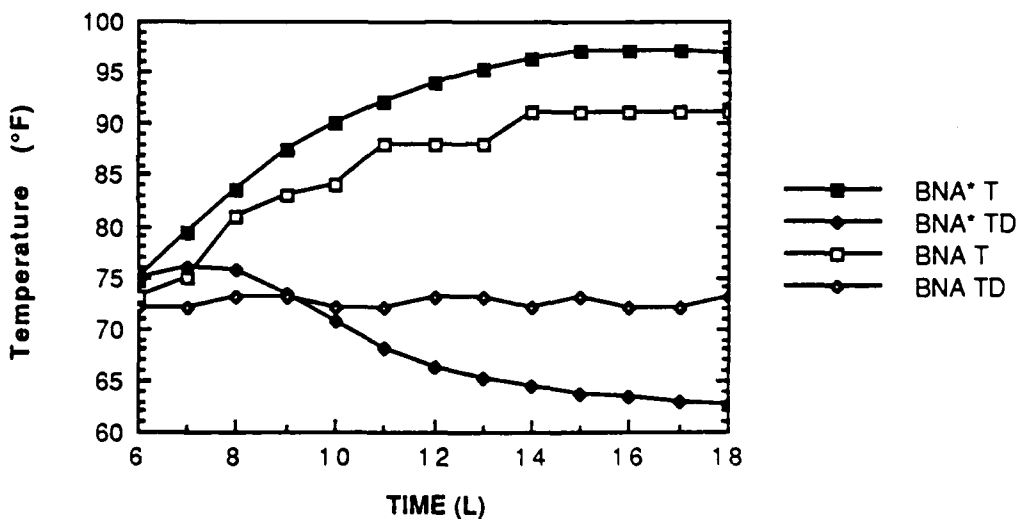
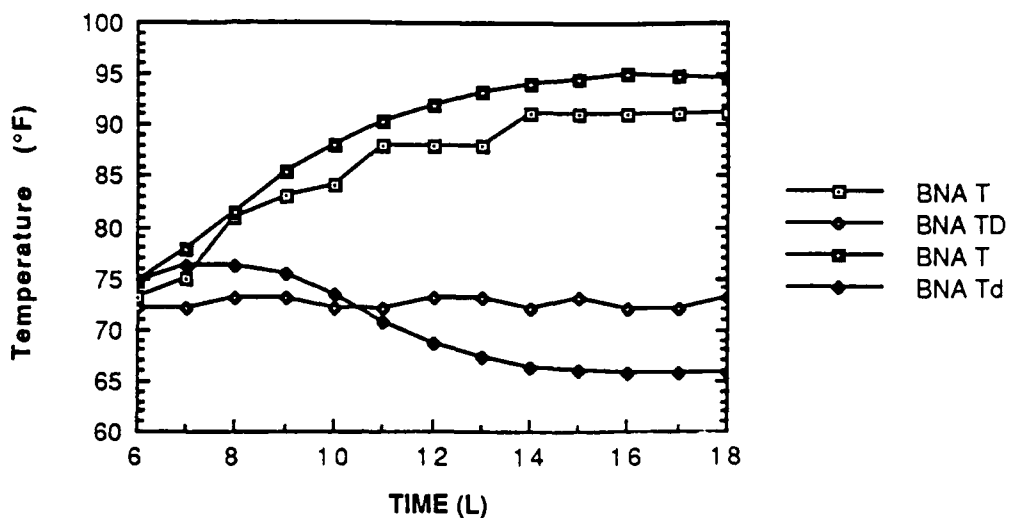


Fig 16. Actual and forecast temperature and dew-point temperature traces for Nashville, Tennessee, 16 July 1986. Top: experiment A, bottom: experiment B. White squares: actual temperature, white diamonds: actual dew-point temperature, black squares: forecast temperatures, black diamonds: forecast dew-point temperatures.

4.3 17 June 1986

The 17 June COHMEX case offers several unique features to examine with the OSU1DPBL model. The first is a weak cold front that was moving through the COHMEX area. Second, Fuelberg et. al. (1990) discovered an area of mesoscale drying that developed during the afternoon over central Tennessee (figure 17). They speculate that this surface dry feature may result from an intrusion of dry air aloft that is seen on water vapor imagery during the same time period. Ruscher and Borland (1990) surmise that this surface dry feature may be the result of dry air from above that becomes entrained in the mixing layer at Nashville, while this drying does not occur at Redstone. This section will give a brief overview of the synoptic situation on 17 June and examine model output to determine if the model can handle this situation. This section will also examine if the model could give clues as to why convective storms did not form until the front was through the Nashville area and will also give the opportunity to examine the PBL on both sides of a front.

4.3.1 Synoptic Overview. A weak cold front associated with a surface low-pressure system centered over eastern Canada was moving south through the COHMEX region (Fig. 18). The 1200 GMT NMC 50 kPa (500 millibar) analysis had a weak short-wave trough just upstream from the COHMEX region. Despite this, the upper level forcing was considered to be weak, and thunderstorms were not forecast to occur during the day. However as the front progressed during the day thunderstorms did form along the Tennessee - Alabama border after 1800 GMT (1300 local).

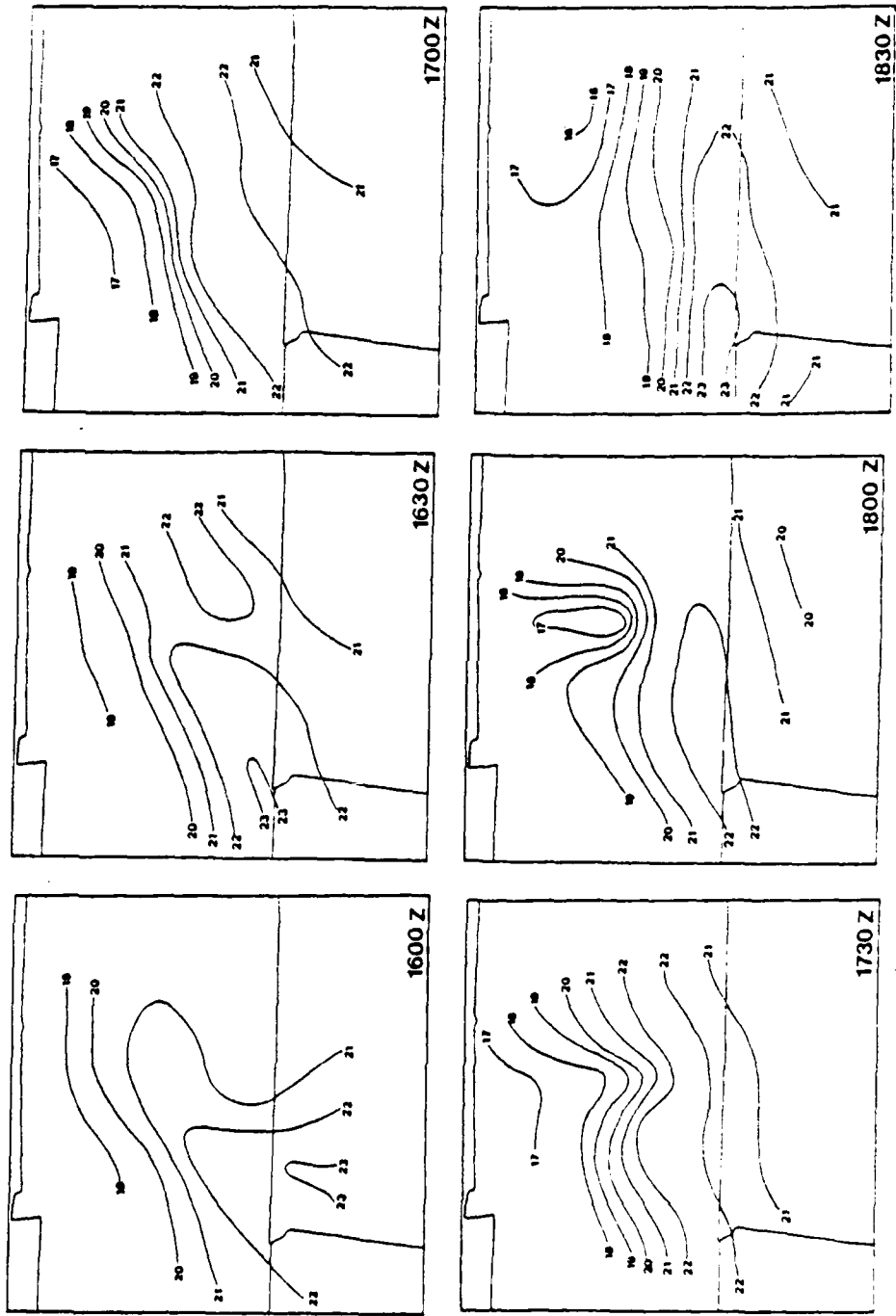


Fig. 17. Surface isotherm analysis (1°C intervals) every 30 min from 1600 to 1830 GMT based on COHMEX data (Schudalla, 1988).

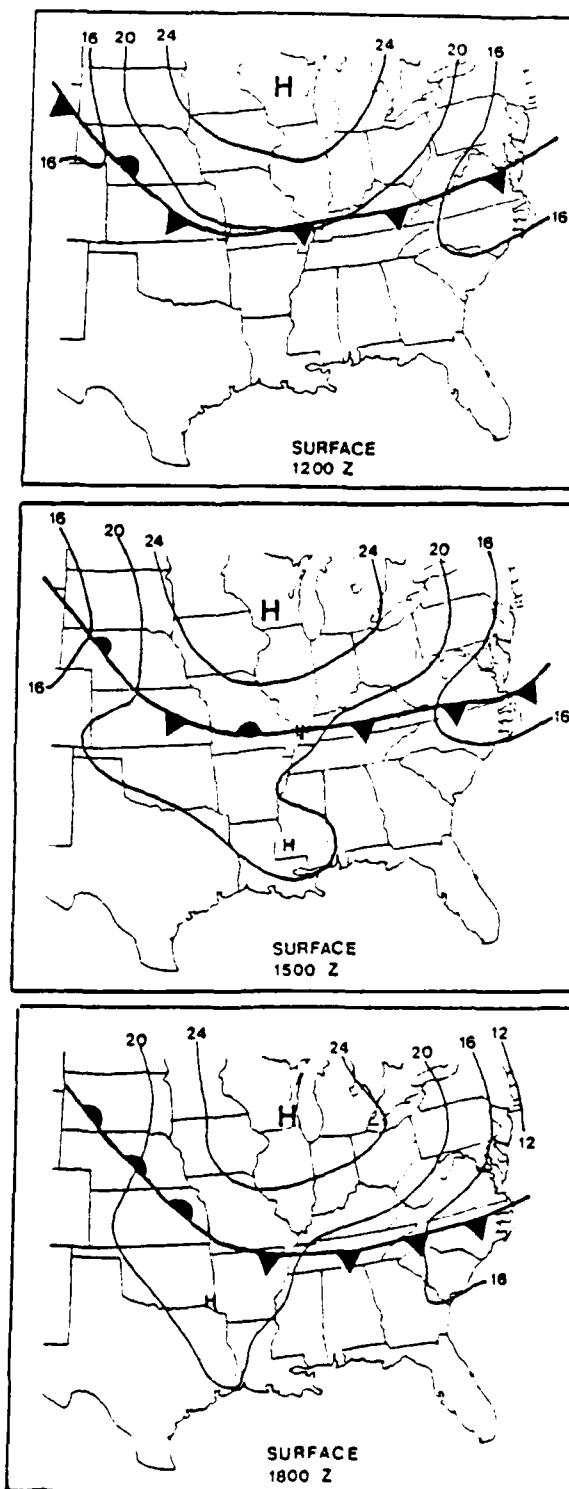


Fig. 18. NMC surface analyses for 1200, 1500, and 1800 GMT 17 June 1986.

4.3.2 Planetary Boundary Layer Height. The planetary boundary layer height forecasts are shown on figure 19. When examining the forecasted growth of the PBL at Redstone, the chief characteristic is the rapid growth of the PBL from 9 local to 10 local from a very stable morning boundary layer. It is important to note that the effects of subsidence and advection from the Bermuda High are neglected in these experiments. Therefore the PBL height forecasts could be overestimated in this case.

The forecasted PBL growth at Redstone in all four runs is fairly uniform from 10 local until 16 local (1500 GMT to 2100 GMT). Here the effects of changing the soil moisture from (0.20, 0.20) in the original run to (0.14, 0.30) for the B, C and D runs becomes noticeable. Where the original run sustains the PBL at 2600 meters, the runs with the different soil moisture values forecast a collapse of the PBL after 1600 local.

The Nashville PBL height forecasts depict a well-mixed early morning PBL with a height of 700 meters. Very little change in PBL forecasts is evident between the runs as the PBL is allowed to gradually grow to 2400 meters.

The difference in the initialized PBL height for BNA and RSA can be attributed to differences in the vertical wind structure. The winds at Redstone are calm at the surface and do not exceed eight knots until 25 kPa (250 millibars). The Nashville winds are 6 knots at the surface and reach 21 knots at 429 meters above the surface. In this case it appears that the model handles these differences in wind profiles correctly to give a realistic initial boundary layer height.

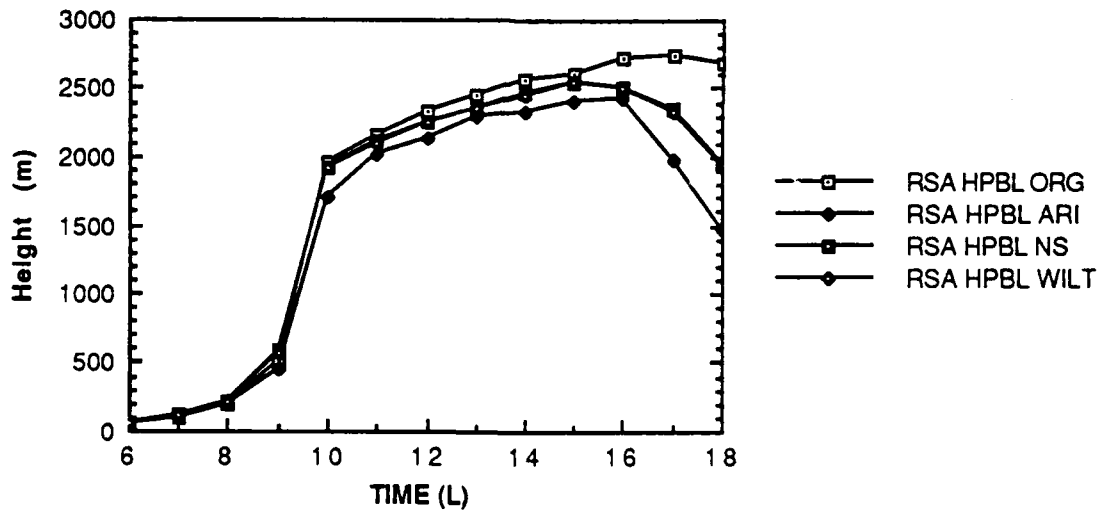
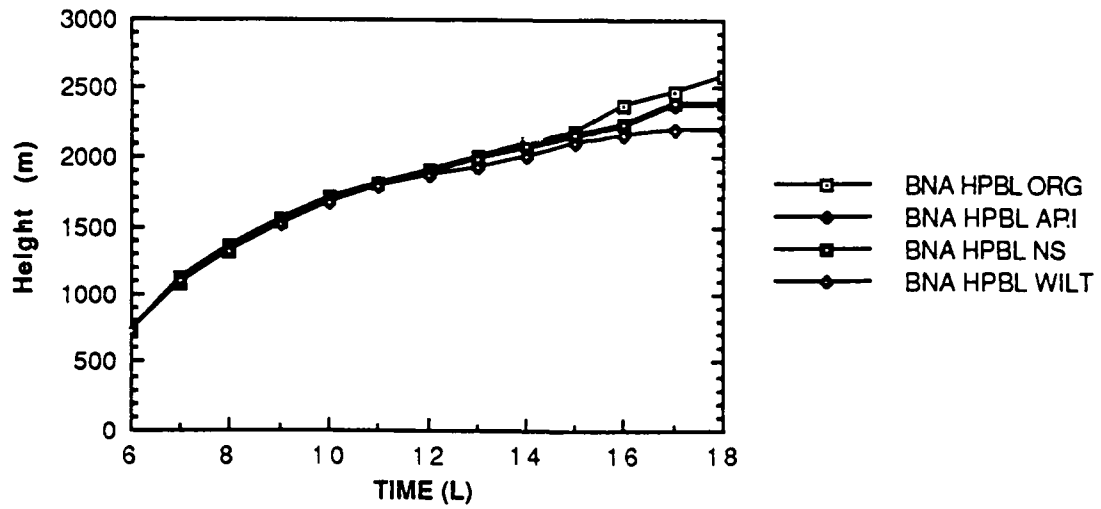


Fig. 19. Forecasted PBL heights for Nashville (top) and Redstone Arsenal (bottom) for 17 June. ORG - experiment A, ARI - experiment B, NS - experiment C, WILT - experiment D.

The model does not permit the Nashville PBL to grow as rapidly nor as high as the Redstone Arsenal PBL, indicating a more stable air mass at Nashville. The rapid growth in the forecast PBL height at Redstone indicates the presence of instability in the form of buoyant air thermals. This agrees well with the 1431 GMT (0931 Local) visible imagery which shows the development of cumulus clouds to the north of Redstone, while clear skies exist at Nashville (Schudalla, 1988). Hence, it appears that the model successfully differentiates between the different air masses found at Redstone Arsenal and Nashville.

4.3.3 Bowen ratio The highest values for Bowen ratios for BNA and RSA are during experiment A (figure 20). Once the new values for soil moisture are used, the value of the Bowen ratios tend more toward Oke's (1978) values mentioned earlier. The interesting finding about the decreased Bowen ratios is that they are influenced by the lower soil layer's WSOIL value than the top soil layer's WSOIL value. For example, the Bowen ratio at RSA drops significantly when WSOIL is changed from (0.20, 0.20), to (0.14, 0.30) respectively; thereby showing the increase in latent heat flux. But perhaps better evidence for this claim can be found in the BNA Bowen ratio. The WSOIL values for BNA are changed from (0.20, 0.20) to (0.11, 0.22); with a value of WSOIL for the top soil layer (0.11) which is lower than the wilting point (0.12) the Bowen ratio still decreases, therefore the latent heat flux must increase given a constant H. So the model is quite sensitive to moisture in the lower soil layer and it is this much thicker lower soil layer where it is most critical to obtain a proper value for soil moisture.

Comparing the Bowen ratios for the B, C and D runs for both stations,

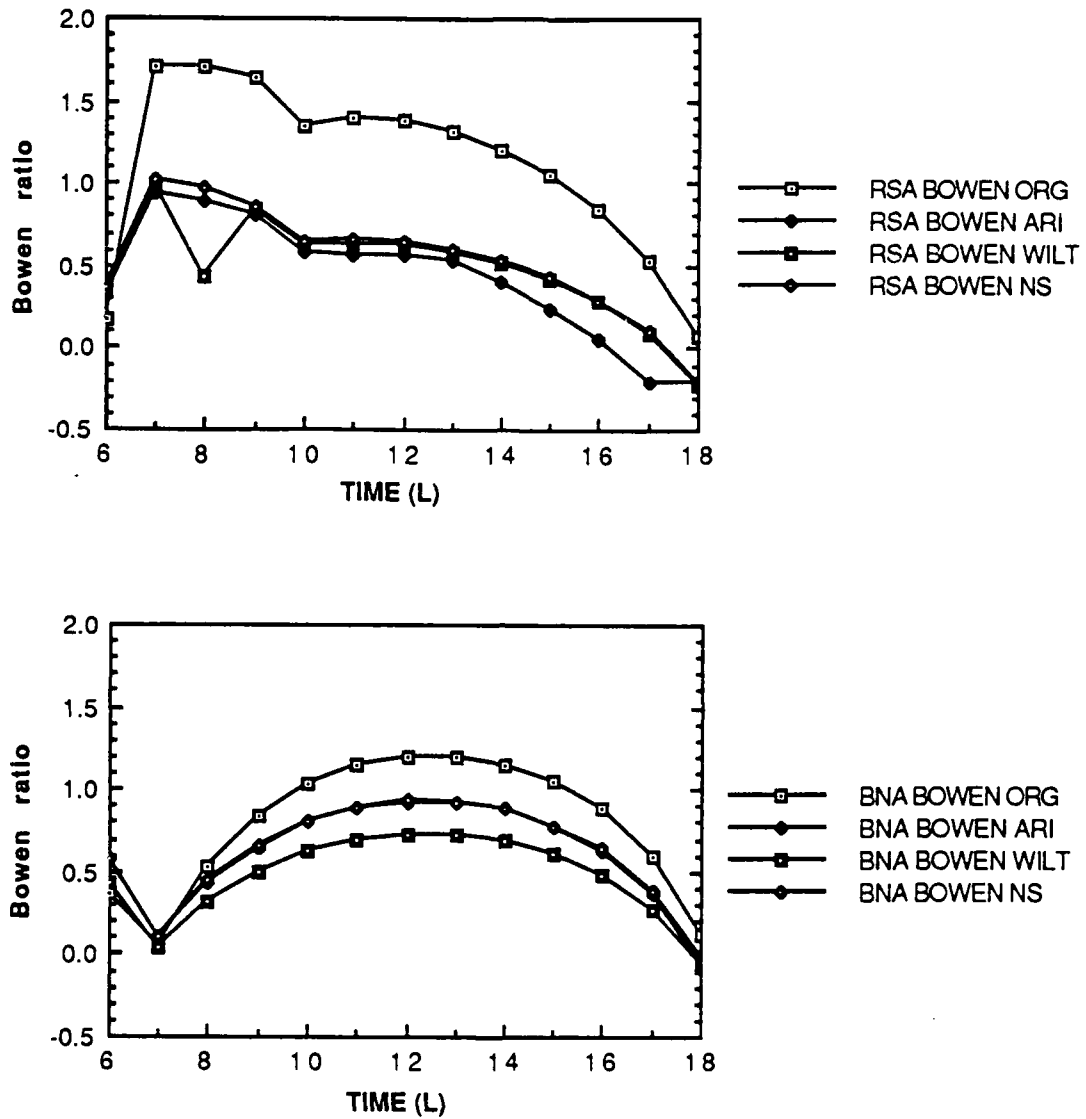


Fig. 20. Bowen ratio for Redstone Arsenal (top) and Nashville (bottom) for 17 June. ORG - experiment A, ARI - experiment B, NS - experiment C, WILT - experiment D.

the ratios for RSA are higher than BNA until 10 local. Apparently, sensible heat flux is larger at RSA than at BNA during the morning, however an examination of the surface energy balance provides more insight to this.

4.3.4 Surface Energy Balance. Based on the more realistic values of Bowen ratio, the surface energy balances of the ARI run were chosen to be examined. Figure 21 depicts the forecast surface energy balance for Nashville and Redstone. Once again the influence of the different soil moisture values is evident. The latent heat flux at RSA is greater than BNA by 1000 local time, while the sensible heat flux is larger at BNA for most of the day. Once again, this appears to be in agreement with the actual conditions that occurred that day as the convection developed over RSA by late morning, while BNA had clear conditions.

4.3.5 Shelter Temperature and Dew-Point Temperature. The actual and forecast T and T_d traces for the ARI run are shown on figure 22. The R^2 values for the forecasts were presented in section 4.1. The same trends that are present in the traces on other days are present in 17 June as well. In both locations, the model does a fine job in forecasting the trend and the actual values for the temperature; the same cannot be said for the dew-point temperature. At RSA, the new values of soil moisture overestimate T_d from 9 local to 15 local, while initially underforecasting the initial value of T_d by 6° F.

At Nashville, a totally different situation exists. It is clearly evident that the derived values of soil moisture do nothing to enhance the models ability to forecast the drying that took place over Nashville. In fact the lack of soil moisture holds the dew-point temperature at 66° F through the entire time

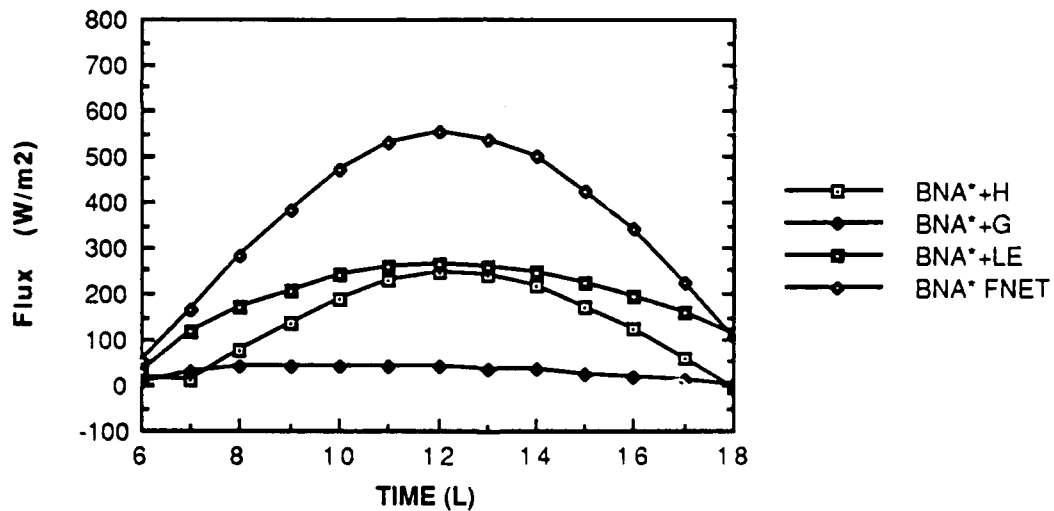
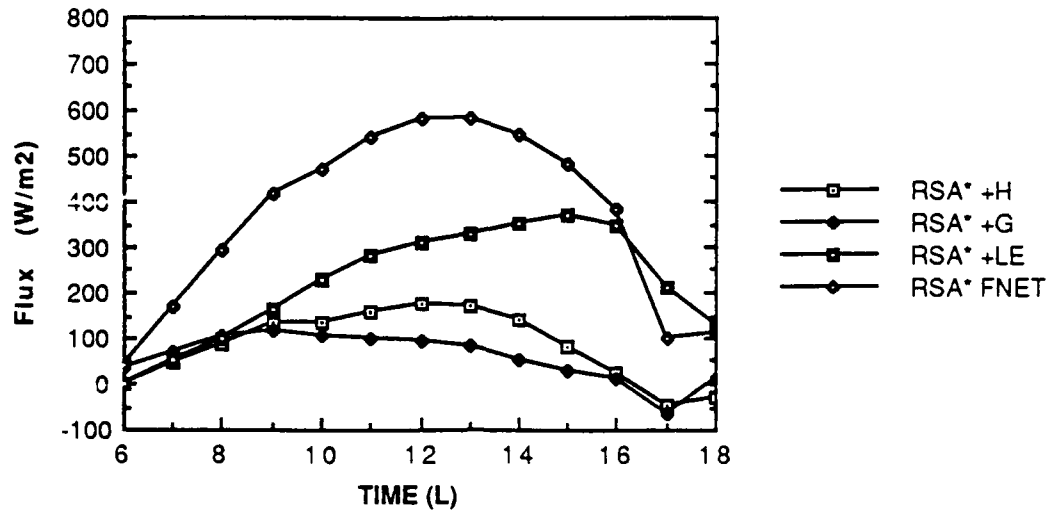


Fig. 21. Surface energy balance for Redstone Arsenal (top) and Nashville (bottom) for 17 June 1986. +H \equiv sensible heat flux (positive upward), +G \equiv soil heat flux (positive downward), +LE \equiv latent heat flux (positive upward), FNET \equiv upward surface radiative flux (positive upward).

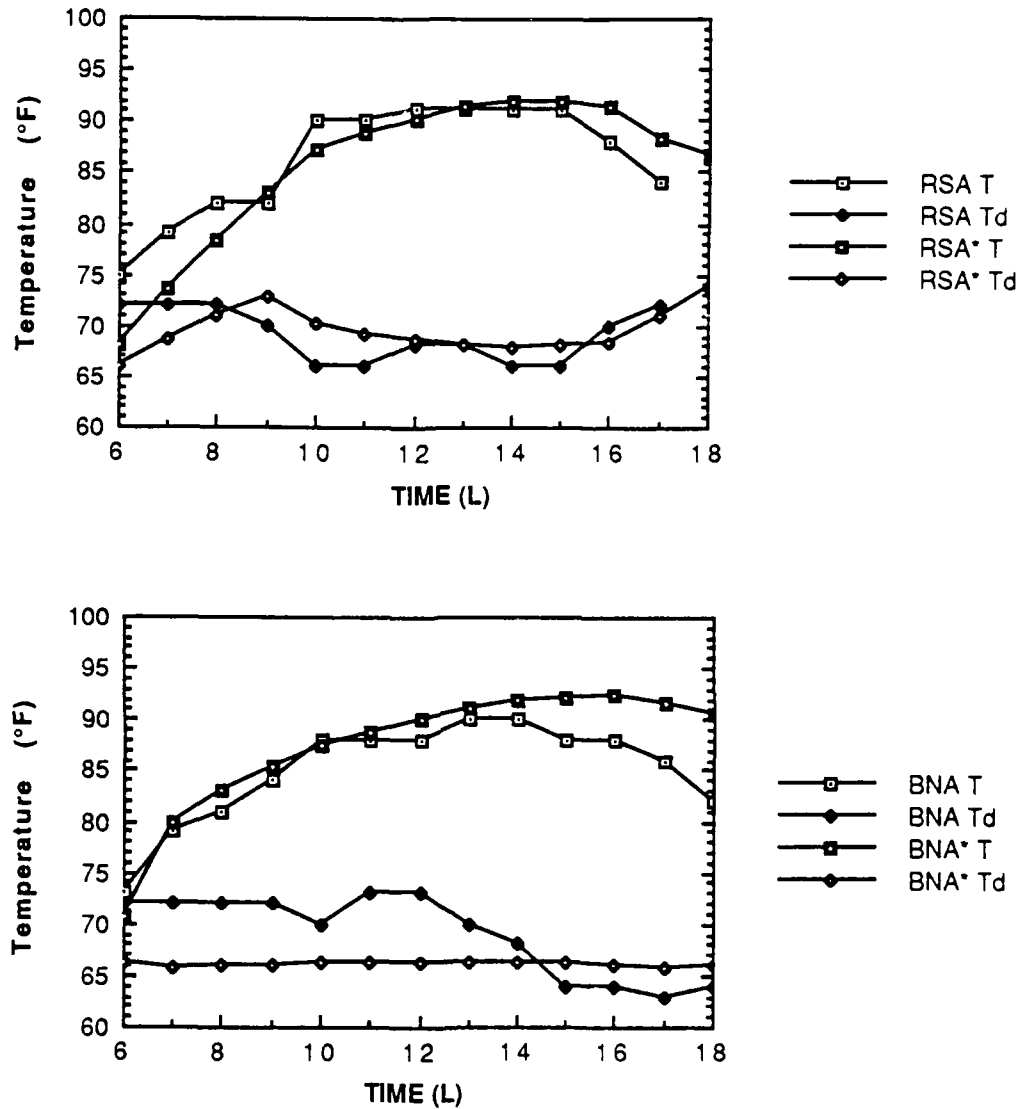


Fig 22. Actual and forecast temperature and dew-point temperature for Redstone Arsenal (top) and Nashville (bottom) for 17 June 1986. RSA T - actual temperature; RSA Td - actual dew-point temperature. RSA* T - experiment B forecast temperature; RSA* Td - experiment B forecast dew-point temperature. BNA T - actual temperature; BNA Td - actual dew-point temperature. BNA* T - experiment B forecast temperature; BNA* Td - experiment B forecast dew-point temperature.

period. One other item to note; the R^2 value for the original run (WSOIL of 0.20,0.20) is 0.679 - which would indicate a good forecast. However, closer inspection of the dew-point traces for experiment A and experiment B shows very little difference in their values (Fig. 23). Here, the slight decrease in forecast T_d for experiment A between 15 and 18 local time follows the trend of the actual dew-point temperature, which leads to the higher value of R^2 . This case also focuses attention on the importance of not relying on statistics alone for forecast verification.

The Nashville case is an example of the weakness of relying solely on a turbulent diffusion model. At Nashville, the model could not accurately predict T_d , as drying took place when the PBL grew into the dry air over Tennessee and entrained this dry air into the PBL. Therefore, for use in an operational setting, the advection of temperature, moisture and momentum must be incorporated into the model. Incorporation of this data may improve forecasts by resolving mesoscale and synoptic scale effects not included in the turbulent diffusion model.

4.4 Boundary Layer Cloud Effects.

An investigation of the boundary layer cloud cover takes place in this section. First, the difference in PBL cloud cover between experiments A and B will be explored. Secondly, the role of cloud cover on the solar radiation will be discussed. The method of calculating cloud cover was covered in section 2.5. It is important to note that only boundary layer clouds are parameterized in

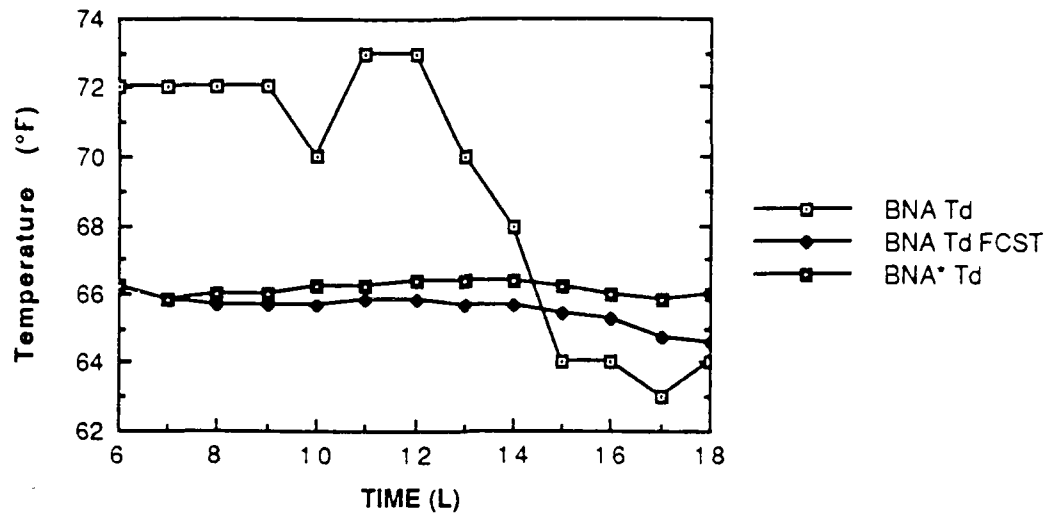


Fig. 23. Comparison of forecasted dew-point temperature runs to actual dew-point temperature for 17 June 1986 at Nashville, Tennessee. BNA Td - actual dew-point temperature; BNA Td FCST - original run dew-point temperature forecast; BNA* Td - ARI dew-point temperature forecast.

the model and the effects of mid and upper-level clouds will be addressed in future studies.

The forecast PBL cloud cover (CLC) for experiments A and B for the three days used in this study are shown on figure 24. Experiments C and D yielded little change in CLC when compared to experiment B, therefore, only A and B will be looked at in this section. The new values of soil moisture in experiment B generally did not lead to a dramatic increase or decrease in the cloud cover over the entire 12 hour forecast run. However, a 10 to 15 per cent decrease in CLC did occur in two cases that will be examined in detail below.

Two cases that deserve closer scrutiny are the 9 June Redstone case and the 16 July Redstone case. Both cases are similar in that the CLC in experiment A is below 10 per cent from 0700 local to 0900 local, then suddenly jumps to about 30 percent at 1000 local time and varies slightly for the rest of the run. This variation should have an impact on the surface energy balance, the question is how much of an impact does it have?

For 9 June (Fig. 25), the difference in cloud cover during the morning is quite evident when comparing the solar radiation, as in experiment A the solar radiation is 150 W m^{-2} greater than experiment B by 0900 local and remains higher for the remainder of the forecast period. A virtually similar situation exists on 16 July (Fig 26). Again, the solar radiation in experiment A is greater than experiment B by 150 W m^{-2} by 0900 local and remains higher than experiment B throughout the rest of the forecast period.

Several cases of a rapid increase or decrease in CLC are also present. These can be seen on 9 June during the Nashville original run at 0800 local

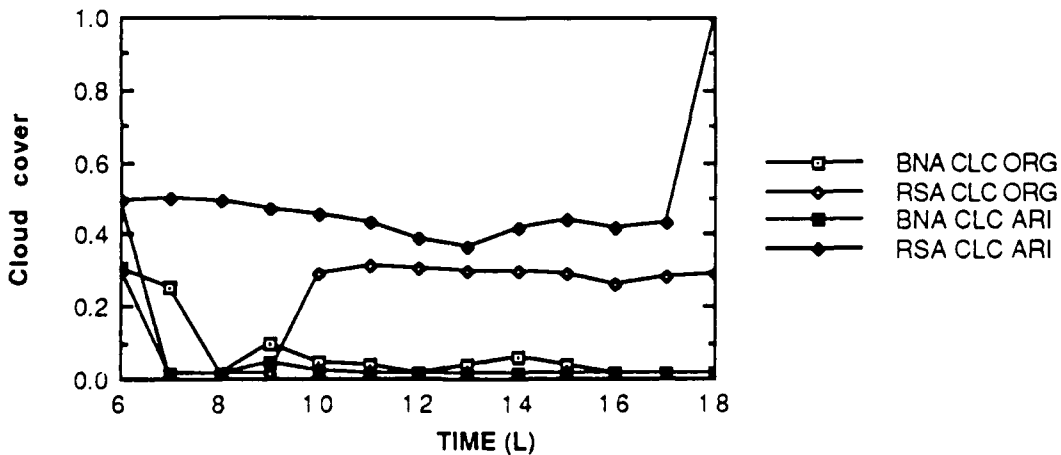
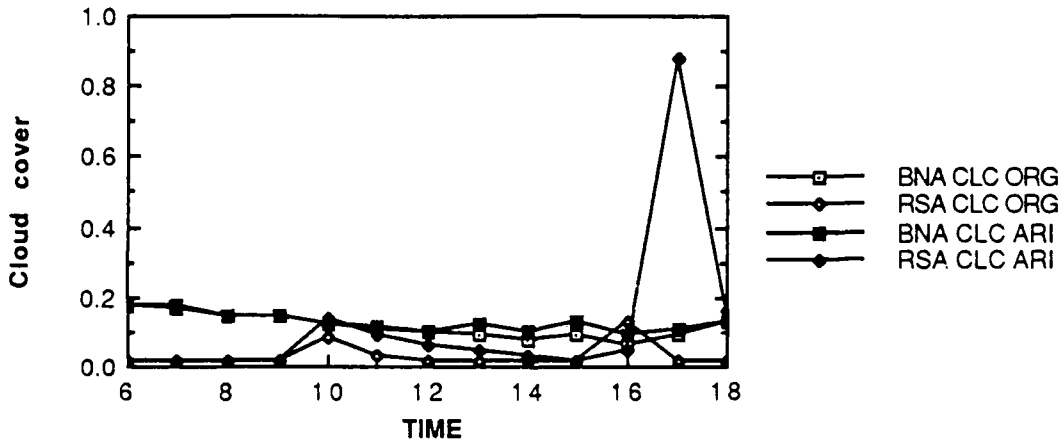
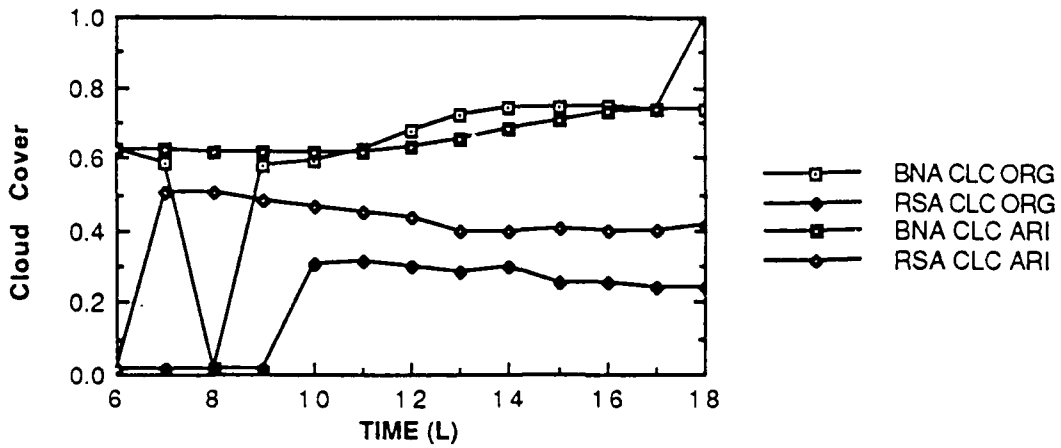


Fig. 24. Forecast PBL cloud cover for 9 June (top), 17 June (center) and 16 July (bottom). BNA CLC ORG; Nashville experiment A cloud cover. RSA CLC ORG; Redstone experiment B cloud cover. BNA CLC ARI; Nashville experiment B cloud cover. RSA CLC ARI; Redstone experiment B cloud cover.

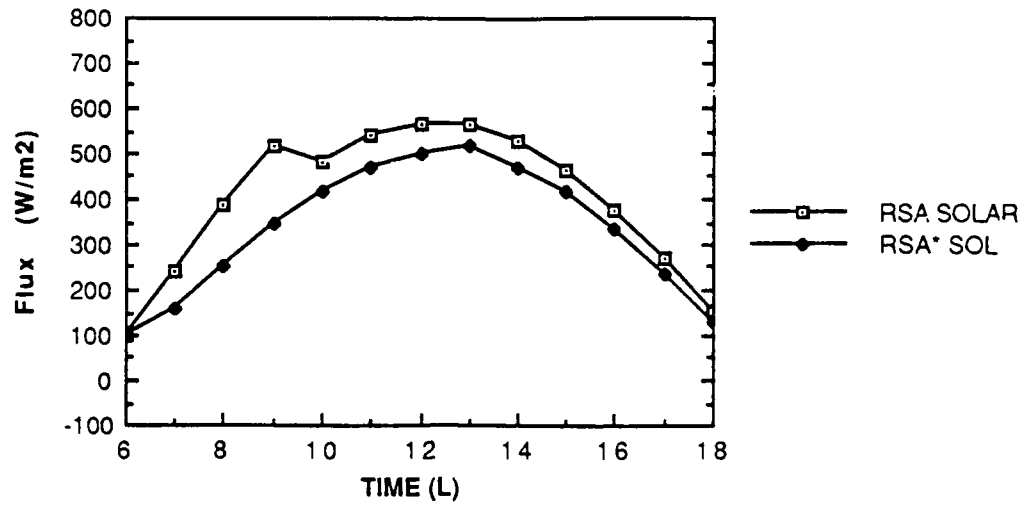


Fig 25. Forecast solar radiation for Redstone Arsenal for 9 June 1986. RSA SOLAR \equiv the solar radiation forecast for experiment A. RSA* SOL \equiv the solar radiation forecast for experiment B.

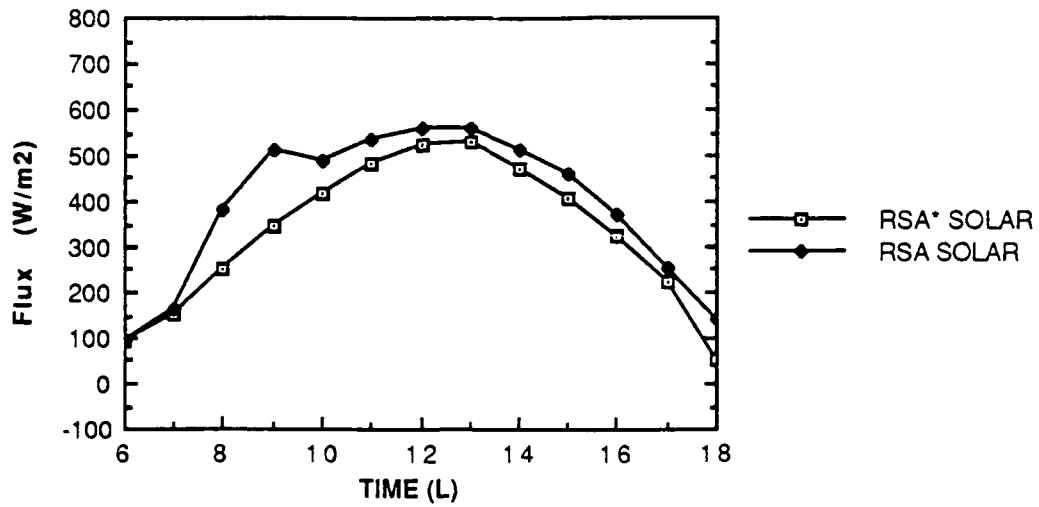


Fig. 26. Forecast solar radiation for Redstone Arsenal for 16 July 1986. RSA SOLAR \equiv the forecast solar radiation for experiment A. RSA* SOLAR \equiv the forecast solar radiation for experiment B.

time and on 17 June at 1700 local time for experiment B at Redstone. During the 17 June Redstone case, the CLC increase leads to a 200 W m^{-2} decrease in solar radiation, while in the 9 June Nashville case the CLC decrease leads to an increase of 150 W m^{-2} in the solar radiation (Fig 27). As the CLC returns to its former level during the next hour, the solar radiation follows a more normal pattern. Despite these sudden jumps in CLC and radiation, a similar jump does not appear in the forecast temperature or dew-point temperature for Nashville on 9 June (Fig. 7, top) or for Redstone Arsenal on 17 June (Fig 22, bottom). The conclusion is while the cloud cover changes can lead to large fluctuations in the solar radiation and the surface energy balance in the model runs, these changes appear to play a minor role in the temperature and dew-point temperature forecasts.

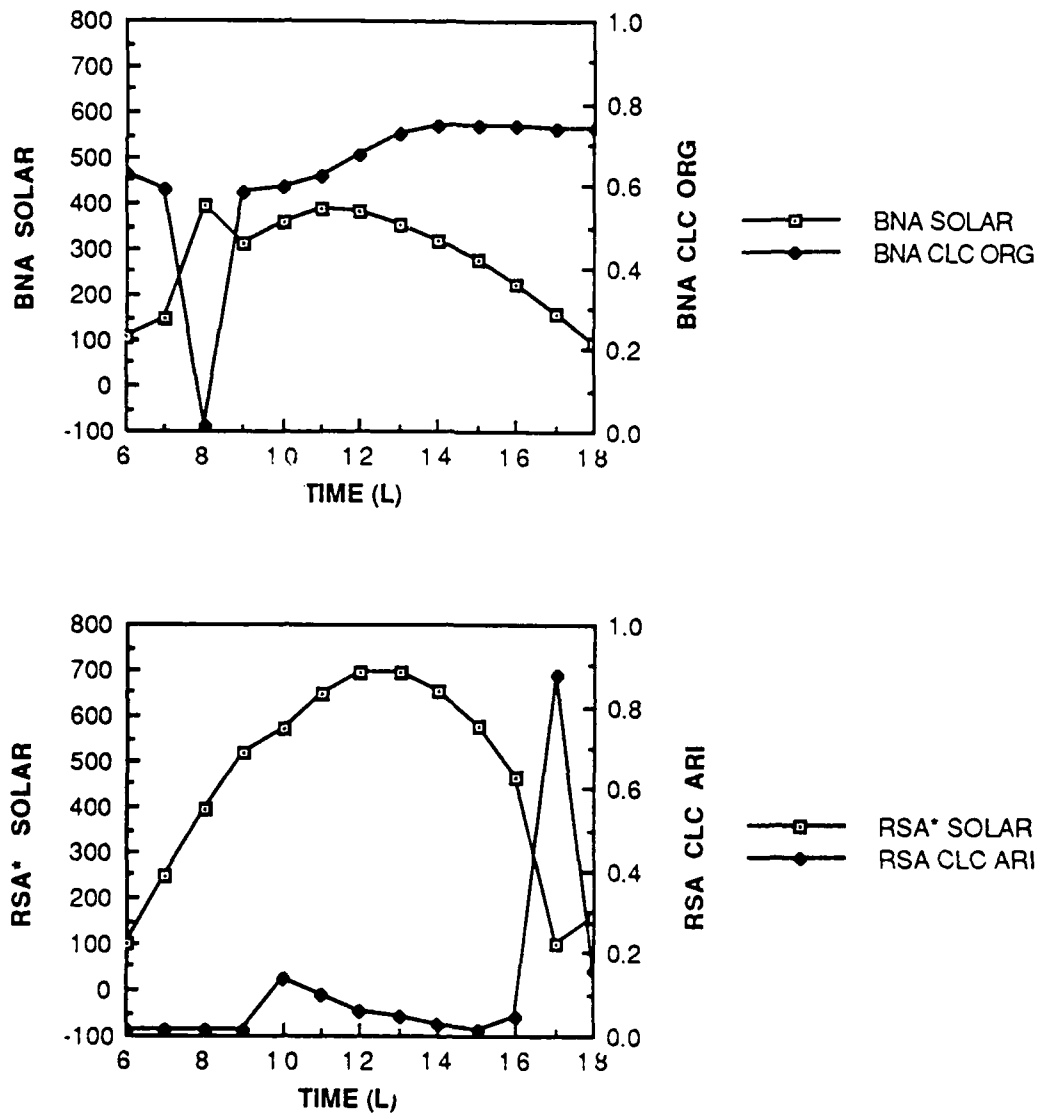


Fig. 27. Forecast values of solar radiation ($W m^{-2}$) (on left ordinate) and PBL cloud cover (on right ordinate) for 9 June at Nashville, Tennessee (top) and 17 June at Redstone Arsenal, Alabama (bottom).

CHAPTER 5

FUTURE IMPROVEMENTS TO MODEL RUNS

Although the results presented here do show promise for using the model for real time applications, there exist several modifications to the data set that may be used to improve the model forecasts.

5.1 Vertical Velocity Calculations

Vertical velocity calculations were not available for use during this work. Therefore, vertical velocity was not used in the input file during any of the experiments. As a result, the effects of large scale subsidence that may have existed over the COHMEX region and limited the growth of boundary layer growth are not represented. However, there is a simple way to calculate vertical velocity for future experiments.

Holton (1979) provides information on deducing the vertical motion by means of the kinematic method. Rather than work through the mathematics by hand, the WXP weather data processing program provides a program for you. For our case, the approximate vertical velocity for the COHMEX region could be found by using the soundings of Nashville, Tennessee (BNA); Centreville,

Alabama (CKL); and Athens Georgia (AHN) (see figure 1, page 29) . While this may not provide the exact vertical velocity over a particular location, it would still be more realistic than to ignore the effects of vertical motion. Table 4 gives an example of the WXP kinematic vertical velocity profile.

5.2 Advection of Moisture, Temperature and Momentum

In chapter two, it was noted that the equations for temperature, moisture and momentum did not include advection terms. As the results section has shown, this could be a limiting factor in the accuracy of forecasting dew-point temperature. Ideally, equations (2), (3) and (4) could be rewritten for use in the model as:

$$\frac{\partial \vec{V}_h}{\partial t} = \frac{\partial}{\partial z} \left(K_m \frac{\partial \vec{V}_h}{\partial z} \right) - w \left(\frac{\partial \vec{V}_h}{\partial z} \right) - \left(\vec{V}_h \cdot \nabla \vec{V}_h \right) \quad (46)$$

$$\frac{\partial \theta}{\partial t} = \frac{\partial}{\partial z} \left(K_h \left(\frac{\partial \theta}{\partial z} - \gamma_\theta \right) \right) - w \left(\frac{\partial \theta}{\partial z} \right) - \left(\vec{V}_h \cdot \nabla \theta \right) \quad (47)$$

$$\frac{\partial q}{\partial t} = \frac{\partial}{\partial z} \left(K_h \frac{\partial q}{\partial z} \right) - w \left(\frac{\partial q}{\partial z} \right) - \left(\vec{V}_h \cdot \nabla q \right) \quad (48)$$

thereby including the effects of advection.

This can be accomplished by using the GDPROF program in the GEMPAK version 4 software that is presently used in the meteorology department at The Florida State University. GDPROF draws a vertical profile at a grid point of diagnostic functions. The benefit of using this program is that a particular latitude, longitude point can be specified for the function that is

desired.

Figures 28, 29 and 30 show how GDPROF can be used for future work. The figure shows a profile of the advection of mixing ratio, temperature and momentum, respectively by the observed wind at Nashville, Tennessee. This information could be used by revising the model code and testing for effectiveness. Incorporation of these profiles might improve forecasts of boundary layer structure due to mesoscale and synoptic scale effects not included in the turbulent diffusion model used in this study. While these profiles may not be able to resolve all mesoscale phenomena that are present, The author feels that inclusion of this data would be a benefit to the original thrust behind this study, i.e. using this boundary layer model to forecast air mass thunderstorms

Table 4. The WXP vertical velocity as computed by the kinematic method on 12 June 1990, 0000 GMT for Nashville, Tennessee; Centreville, Alabama and Athens, Georgia. Units of pressure in millibars, vorticity and divergence are 10^{-5} per second and vertical motion is in negative microbars per second. Note: no upper boundary condition has been applied here.

Level	Pressure	Vorticity	Divergence	Vertical motion
1	968.5	-0.009	-0.514	
	950.0			0.190
2	925.0	0.270	-0.316	
	900.0			0.348
3	875.0	-0.159	-0.357	
	850.0			0.526
4	825.0	-0.399	0.270	
	800.0			0.391
5	775.0	0.148	-0.734	
	750.0			0.758
6	725.0	0.769	-1.408	
	700.0			1.462
7	675.0	0.590	-1.240	
	650.0			2.082
8	625.0	0.189	-1.618	
	600.0			2.891
9	575.0	-0.180	-2.032	
	550.0			3.907
10	525.0	-1.423	-1.540	
	500.0			4.677
11	475.0	-3.171	-0.547	
	450.0			4.950
12	425.0	-2.036	-0.660	
	400.0			5.280
13	375.0	-0.541	-1.307	
	350.0			5.934
14	325.0	-3.060	-1.207	
	300.0			6.537
15	275.0	-4.968	-0.758	
	250.0			6.916

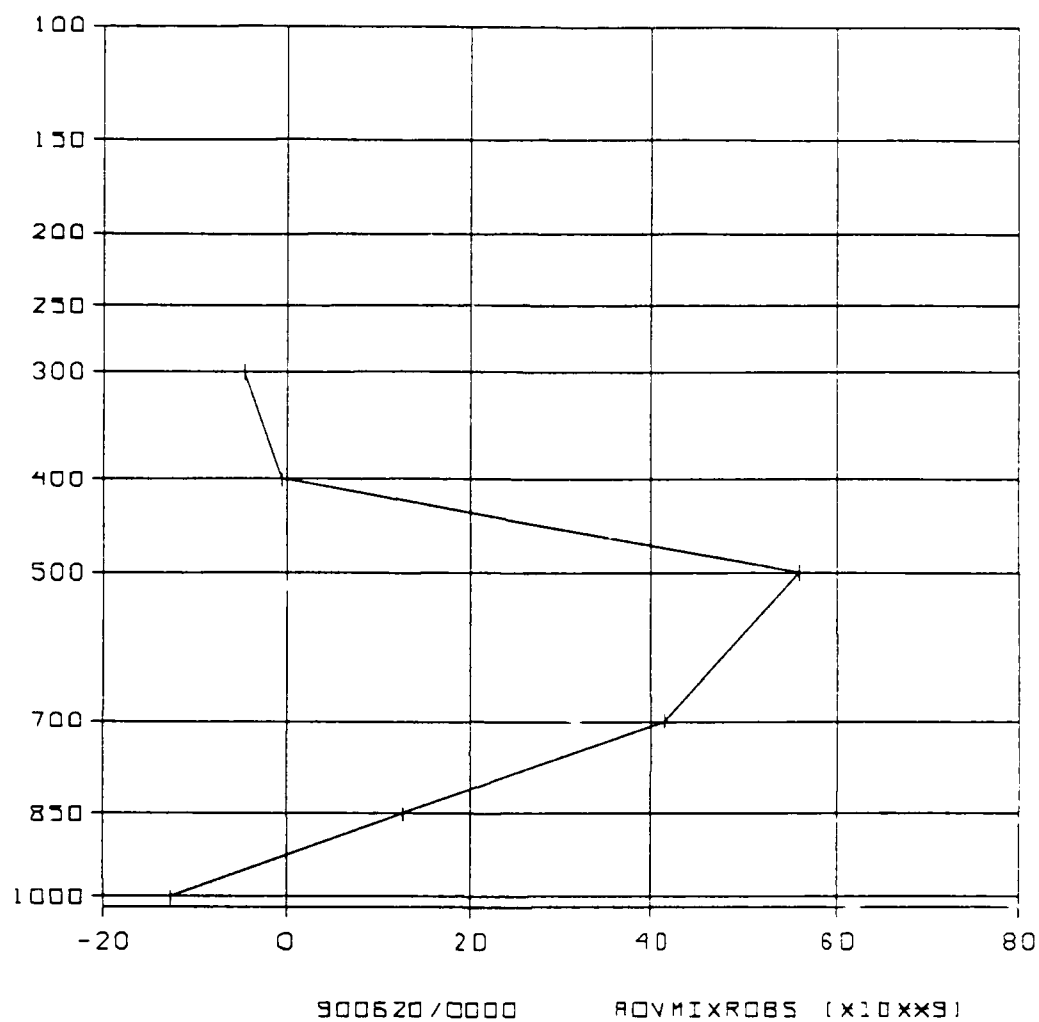


Fig. 28. Vertical profile of the advection of mixing ratio (g/Kg) by the observed wind at 36.2° north, 86.7° west (Nashville, Tennessee) as computed by the GDPROF program of the GEMPAK meteorological data display system. Units of the advection are s^{-1} . Ordinate is pressure (hPa).

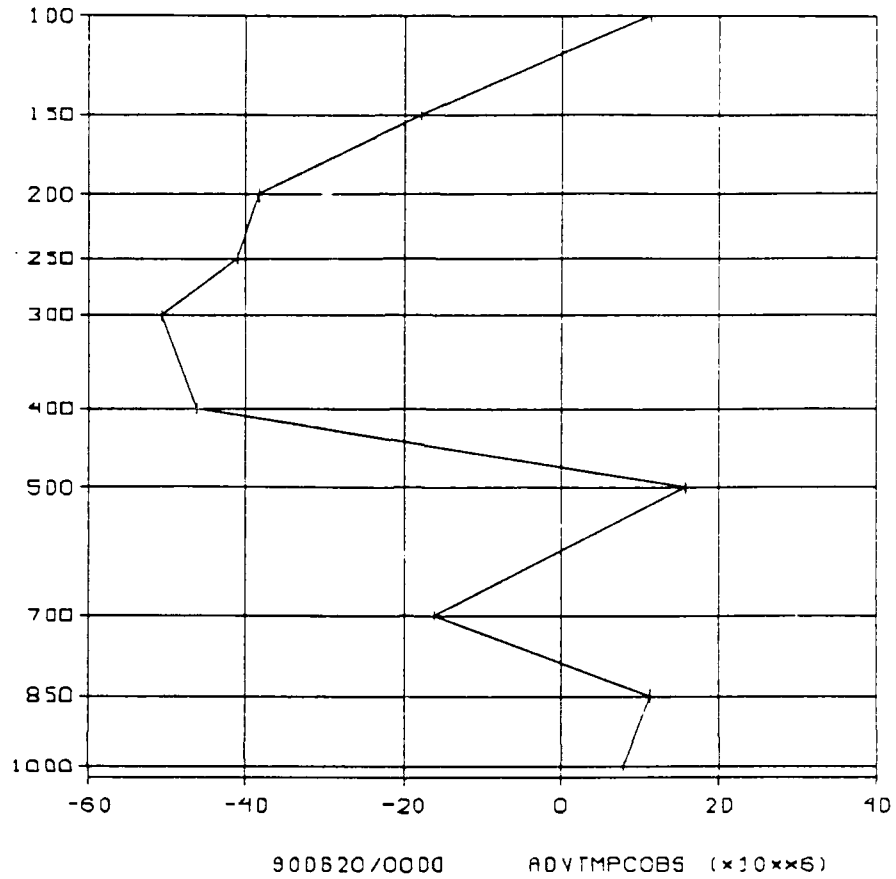


Fig. 29. Vertical profile of the advection of temperature ($^{\circ}\text{C}$) by the observed wind at 36.2° North, 86.7° west (Nashville, Tennessee) as calculated by the GDPROF program of the GEMPAK meteorological data display system. Units of advection are $^{\circ}\text{C s}^{-1}$. Ordinate is pressure (hPa).

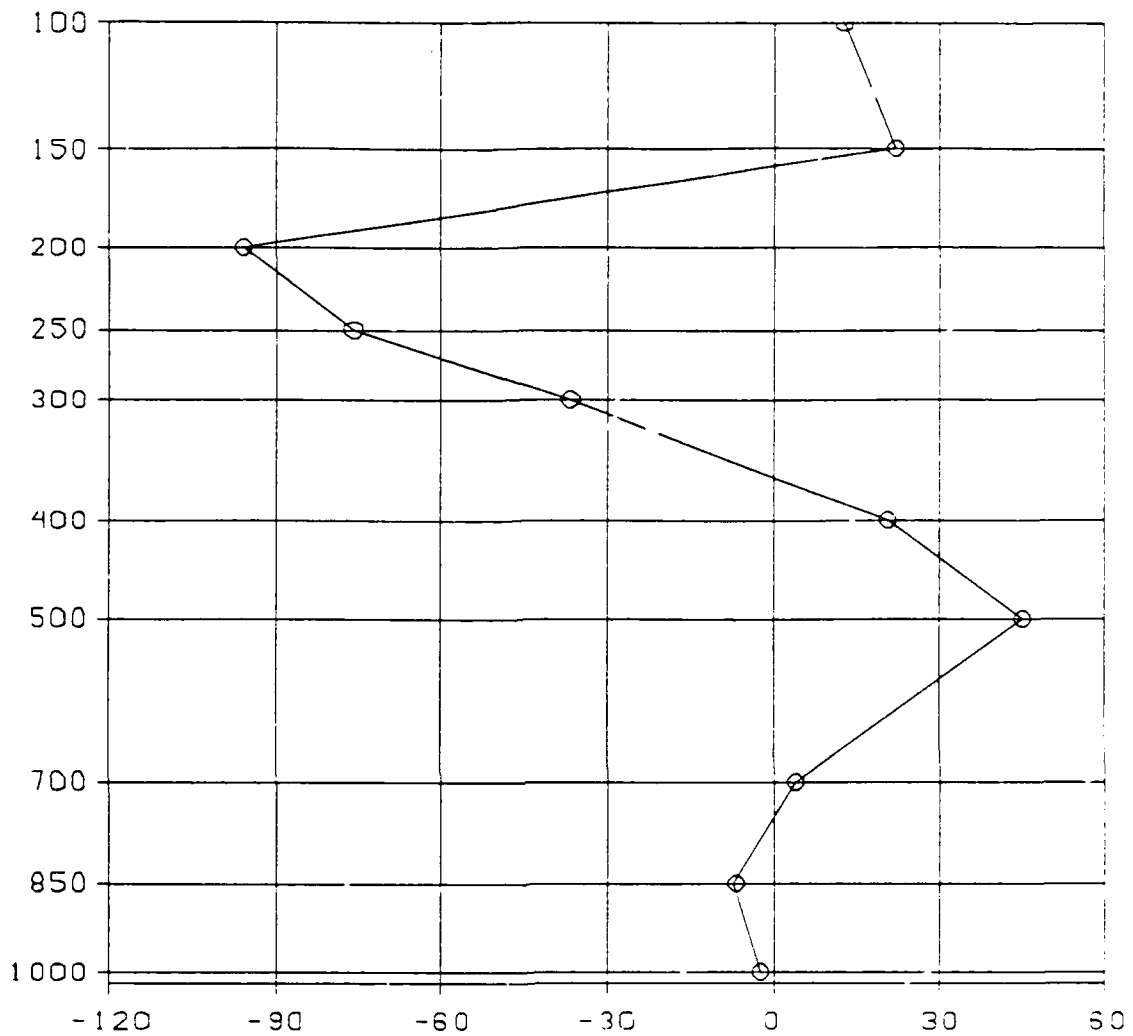


Fig. 30. Vertical profile of the advection of momentum (u component of wind) by the observed wind at 36.2° north, 86.7° west (Nashville, Tennessee) as calculated by the GDFPROF program of the GEMPAK meteorological data display system. Units of advection are m s^{-1} . Ordinate is pressure (hPa).

CHAPTER SIX

CONCLUSION

An investigation of the forecasting capabilities of a one-dimensional planetary boundary layer model has been made examining three days that occurred within the Cooperative Huntsville Mesoscale Experiment (COHMEX).

The introduction of this work discussed the potential of the model to forecast air-mass thunderstorms. No thunderstorm forecasting is actually performed during this work. However, the investigation into the models capabilities to forecast various boundary layer and surface layer parameters (i.e. temperature, dew-point temperature, planetary boundary layer height) provides results that are encouraging enough to continue further testing with this model.

Perhaps the most important aspect of this research was the development and application of an antecedent retention index (ARI). Early results indicated soil moisture had a significant influence and research was done to devise a simple yet effective way of computing soil moisture. While soil moisture is highly variable temporally and spatially, the author feels that the method used in this work is more accurate than simply guessing the soil moisture value, based on the results presented here.

R^2 scores were examined to determine how well the model predicted T and T_d for a 12 hour period. While the results of the temperature forecasts were very good, the dew-point temperature forecasts were often poor. A closer examination of the R^2 scores reveals that several good values of R^2 were significantly biased (i.e., a 4 °C overestimate of temperature in one case); indicating that analysis should not rely on only one statistic. The best R^2 results were obtained when the soil moisture was replaced with the ARI value, the soil type was changed to clay and the wilting point was lowered.

Results from the 9 June and 16 July cases were examined to determine if large fluctuations in forecast PBL height between the model runs indicated better forecasts for T and T_d . These tests were inconclusive. Rapid changes in the boundary layer cloud cover were also investigated. While these fluctuations did have an effect on the surface energy balance for a brief period of time, they were found to have little impact on T and T_d forecasts.

Fluctuations in the Bowen ratio due to changes in the soil moisture were also examined. It was found that changes in the soil moisture had substantial influence upon the surface energy balance and hence, the Bowen ratio. In five of the six cases examined, the inclusion of soil moisture resulted in Bowen ratios in closer agreement with Oke's values of 0.4 to 0.8.

The 17 June 1986 COHMEX case was examined in detail. The model was able to differentiate between air masses on both sides of the front at Nashville, Tennessee and Redstone Arsenal, Alabama. This would be important to future applications of air mass thunderstorm forecasting over the southeastern United States, particularly in the event of an outflow boundary

stabilizing the air over one location but not another.

Future improvements to the model could include the use of data from the GEMPAK and WXP meteorological data display systems. From these systems, data can be included such as vertical velocity and the advection of temperature, moisture and momentum. Revision of the model to incorporate this data may help to resolve mesoscale phenomena such as the drying that was seen over Nashville, Tennessee for the 17 June 1986 case.

The author recognizes that for the purpose of thunderstorm forecasting, the best situation would be for a mesoscale surface observation and sounding network to take advantage of the models capabilities. Among the advantages of this model are that it is programmed in standard FORTRAN and will run on a standard personal computer in a matter of several minutes. This model may provide a weather station a low cost method to determine stability and convective potential over certain regions where VAS retrievals may not be available.

APPENDIX

MODEL DEFAULT PARAMETERS

Vertical grid resolution:	38 levels
Time step:	600 seconds
Duration of model run:	12 hours
P power in K profile	2
Critical Richardson number:	0.5
Roughness length for momentum:	0.1 meters
Roughness length for heat:	0.1 meters
Surface albedo:	0.23
Fractional cloud cover:	0.0
Precipitation parameters:	0.0
Soil type:	sandy clay loam
Wilting point:	0.12
Shading factor:	0.7
Air dry value:	0.25
Number of soil layers:	2
Number of geostrophic wind observations	2

REFERENCES

- Bennett, H. H., 1921: *Soils and Agriculture of the Southern States*. The MacMillan Company, New York
- Bjerknes, J. and E. Palmén, 1937: Investigations of selected European cyclones by means of serial ascents, *Geofysica Publika*, **12**, 5-62.
- Brenner, S., C.-H. Yang, and K. Mitchell, 1984: The AFGL Global Spectral Model: Expanded Resolution Baseline Version. Rept. No. AFGL-TR-84-0308, Air Force Geophysics Laboratory, Hanscom AFB, 72 pp. [ADA160370]
- Businger, J. A., J. C. Wyngaard, Y. Izumi, and E.F. Bradley, 1971: Flux-profile relationships in the atmospheric surface layer. *J. Atmos. Sci.*, **28**, 181-189.
- Ek, M. and L. Mahrt, 1989: *A User's Guide to OSU1DPBL version 1.0.3*, Department of Atmospheric Sciences, Oregon State University, Corvallis, 106 pp.
- Fawbush, W. J. and R. C. Miller, 1952: A mean sounding representative of the tornadic airmass environment, *Bull. Amer. Meter. Soc.*, **33**, 303-307.
- Fuelberg, H. E., R. L. Schudalla and A. R. Guillory, 1989: Mesoscale analysis of a pre-convective environment. *Wea. and Forecasting*, submitted
- Hoke, J. E., N. A. Phillips, G. J. DiMego, J. J. Tuccillo and J. G. Sela, 1989: The regional analysis and forecasting system of the National Meteorological Center, *Wea. and Forecasting*, **4**, 323-334.

- Holton, J. R., 1979: *An Introduction to Dynamic Meteorology*. Academic Press, New York, 391pp.
- Holtstag, A. A. M. and A. C. M. Beljaars, 1988: Surface flux parameterization schemes; developments and experiences at KNMI. ECMWF Workshop on Parameterization of Fluxes and Land Surfaces, 24-26 Oct., 1988, p. 121-147, Reading, England.
- Holtstag, A. A. M. and H. A. R. de Bruin, 1988: Applied modeling of the nighttime surface energy balance over land. *J. Appl. Meteorol.*, **27**, 689-704.
- Louis, J. -F., 1979: A parametric model of vertical eddy fluxes in the atmosphere. *Bound.-Layer Meteorol.*, **17**, 187-202.
- Mahrt, L., 1987: Grid-averaged surface fluxes. *Mon. Wea. Rev.*, **115**, 1550-1560.
- Mahrt, L. and H.-L. Pan, 1984: A two-layer model of soil hydrology. *Bound.-Layer Meteorology.*, **29**, 1-20.
- McGinley, J., 1986: *Mesoscale Meteorology and Forecasting*, (P.S. Ray, Ed.), Amer. Meteor. Soc., Boston, Massachusetts, 657-688.
- Pan, H. -L. and L. Mahrt, 1987: Interaction between soil hydrology and boundary layer development. *Bound.-Layer Meteorol.*, **38**, 185-202.
- Panofsky, H. A. and G. W. Brier, 1968: *Some Applications of Statistics to Meteorology*. The Pennsylvania State University, University Park, Pennsylvania, 224 pp.
- Oke, T. R., 1978: *Boundary Layer Climates*. Methen press, London, 372 pp.

- Ruscher, P. H. and T. J. Borland, 1990: A boundary layer model for short-range weather forecasting. *Preprints, 3rd Workshop in Operational Meteorology*, Montréal, Canada; Canadian Meteor and Oceano. Soc., 312-316.
- Ruscher, P. H., 1988: Parameterization of the very stable boundary layer in a simple model. *Preprints, Eight Symposium on Turbulence and Diffusion*, San Diego Ca; Amer. Meteor. Soc., 299-301.
- Saxton, K. E., and A. T. Lenz, 1967: Antecedent retention indexes predict soil moisture. *J. Hydraul. Div., ASCE*. **93**, 223-241.
- Schudalla, R. L., 1988: A case study of thunderstorm development on 17 June 1986 during COHMEX. M. S. thesis, Department of Meteorology, The Florida State University, Tallahassee, 99 pp.
- Schulz, E. F., 1973: *Problems in Applied Hydrology*. Water Resources Publications, Fort Collins, Colorado.
- Troen, I. and L. Mahrt, 1986: A simple model of the atmospheric boundary layer: sensitivity to surface evaporation. *Bound.-Layer Meteorol.*, **37**, 129-148.

BIOGRAPHICAL SKETCH

Captain Thomas J. Borland [REDACTED]

[REDACTED] After graduating from the State University of New York (SUNY) at Farmingdale in 1981 with an Associate of Arts in Liberal Arts, Captain Borland transferred to the University of Oklahoma and graduated in May, 1984 with a Bachelor of Science in Meteorology. Captain Borland was commissioned a second lieutenant after completing the U.S. Air Force Officer Training School in August of 1984. Captain Borland was the assistant staff weather officer at Ft. Rucker, Alabama from September of 1984 to October of 1985. From there he became the assistant staff weather officer to U.S. Special Operations Command at MacDill Air Force Base, Tampa, Florida from October, 1985 to August, 1988. Upon being accepted to the Air Force Institute of Technology (AFIT), Captain Borland then came to The Florida State University. Captain Borland is a member of Chi Epsilon Pi, the national meteorological honor society and is co-author with Dr. Paul Ruscher of the article 'A Boundary Layer Model for Short-Range Weather Forecasting' published in the pre-prints of the *3rd Workshop on Operational Meteorology*.